Spring 2019

Synthesis and Characterization of Tripodal Tris(nitroxide) Aluminum, Gallium, and Indium Complexes

Audra J. Woodside , '19

Synthesis and Characterization of Tripodal Tris(nitroxide) Aluminum, Gallium, and Indium Complexes

Senior Course Thesis

Audra J. Woodside
Department of Chemistry and Biochemistry Swarthmore College
May 2019
Advisor: Christopher R. Graves

Part of this thesis appears in: Woodside, A.J.; Smith, M.A; Herb, T.M.; Mano, B.C.; Carroll, P.J. Rablen, P.R.; Graves, C.R. Synthesis and Characterization of a Tripodal Tris(nitroxide) Aluminum Complex and Its Catalytic Activity toward Carbonyl Hydroboration. *Organometallics* **2019**, *38* (5), 1017-1020.

Table of Contents

Acknowledgements

First, I would like to thank Professor Chris Graves for investing so much time and energy into helping me grow as a chemist. It is only through his help that this work was made possible. He taught me so much both in lab and in life; I would not be where I am today without his constant support and guidance.

I would also like to thank my fellow lab members: Scout Clark, Lucas Heinzerling, Judah Raab, Mika Maenaga, Henry Wilson, and particularly Mackinsey Smith for their friendship and support throughout my time in the Graves lab. Whether I needed a liquid nitrogen buddy or someone to bounce ideas off of, they were always there for me. Additionally, I would like to acknowledge Thomas Herb from Albright College, who built the foundations of this project, as well as the Schelter group for their generous help with the synthesis of our ligand. I am very thankful for the collaborators at the University of Pennsylvania for their assistance in the characterization of our compounds via X-ray diffraction.

I also have to thank the members of the Department of Chemistry and Biochemistry of Swarthmore College. I am so thankful to have had the opportunity to learn from you over the past four years.

Finally, I would like to thank my parents for giving me the opportunity to attend Swarthmore College, and my family and friends for their unwavering support throughout this journey.

Abstract

One important challenge in green chemistry is the development of safe and sustainable catalytic systems for molecular transformations that do not rely on precious metals. In this vein, I explore how one can expand the utility of aluminum complexes. Aluminum is a prime choice for such catalytic development as it is relatively inexpensive (less than $2/kg), readily available, and non-toxic. Although there are ample examples of aluminum complexes acting as Lewis-acid catalysts, the lack of readily accessible multi-electron redox states leaves aluminum complexes inept in redox-based transformations. In order for aluminum complexes to be used in redox reactions, I prepared complexes that contain redox-active ligands.

Specifically, I focused on the synthesis of aluminum complexes implementing a multidentate ligand incorporating three nitroxide (N-O) functional groups, which is known to exist across three oxidation states. It is hypothesized that the Al-nitroxide complex will similarly span several oxidation states. Herein, I report the synthesis ($TriNOx^{3-}$)Al-py, which uses a multidentate redox-active tripodal tris(nitroxide) ligand. Moreover, I report the synthesis of analogous gallium and indium complexes, providing an array of complexes that vary in electronic parameters, steric profiles, and metal ionic radius. The aluminum complex exhibits multi-electron electrochemical behavior, and has the ability to participate in metal-ligand cooperative catalysis due to the Lewis acidity of the aluminum center and the Lewis basicity of the nitroxide nitrogens. These characteristics have been exploited in a catalytic system for the hydroboration of carbonyls. Such use of the aluminum complex represents new transition-metal-like reactivity for an earth-abundant metal.

List of Common Abbreviations

DCM = dichloromethane

Dipp = 2,6,-Diisopropylphenyl

HBpin = pinacolborane

MeCN = acetonitrile

$NaN(SiMe_3)_2$ = sodium bis(trimethylsilyl)amide

NNN = bis(2-isopropylamino-4-methoxyphenylamine

N-O group = nitroxide functional group

($^{R}pyNO^{-}$) = *N*-*tert*-butyl-*N*-(2-(5-R-pyridyl))nitroxyl, R = H, CH_3, CF_3)

Py = pyridine

THF = tetrahydrofuran

($TriNOx^{3-}$) = $[\{(2\text{-}^{t}BuNO)C_6H_4CH_2\}_3N]^{3-}$

1. Introduction

An important challenge in green chemistry is the development of safe and sustainable catalytic systems for molecular transformations that do not rely on precious metals.[1] Such systems increase the sustainability of a reaction by reducing the cost, material, and energy needed to obtain a product. Aluminum is a prime choice for such catalytic development as it is readily available (making up more than 8% of the earth's crust),[2] non-toxic, and relatively inexpensive. At less than $2.00/kg, aluminum is significantly less expensive than precious metals such as platinum (~$38,000/kg) and palladium (~$24,000/kg).[3] Aluminum is also less expensive than numerous first row transition metals such as copper (~$6.00/kg), cobalt (~$30.00/kg), and nickel (~$13.00/kg), which are often thought of as better economic alternatives to precious metals.[3] Thus, not only is the development of aluminum catalysts environmentally friendly, but there is also a large economic motive.

Aluminum is known to be stable in the 3+ oxidation state, and numerous examples of aluminum complexes acting as Lewis-acid catalysts exist. For instance, $AlCl_3$ is famously used to catalyze Diels-Alder reactions,[4] Friedel-Crafts alkylations,[5] Cl/F exchange reactions,[6] and the halogenation of aromatic groups.[7] Additionally, aluminum alkoxides catalyze Meerwein-Ponndorf-Verley reductions.[8] Although aluminum readily catalyzes the above reactions, the lack of easily accessible multi-electron redox states leaves aluminum complexes inept in redox-based reactions. A potential way to expand the utility of aluminum is to complex the element with redox-active and/or non-innocent ligands. In such instances, the compound can participate in redox events independent of changes in metal oxidation state.[9] Redox non-innocent

ligands can be involved in reactivity in two ways: (1) the redox-active ligand participates in the catalytic cycle by accepting or donating electrons (2) the ligand participates by forming and/or breaking substrate covalent bonds.[10] The formation of a redox-active aluminum complex results in a compound that can coordinate substrates through its Lewis acidity as well as activate those molecules via either redox properties or more classic organic-type chemistry.

The development of redox-active ligand metal complexes has expanded the reaction profiles of transition,[11,12,13]main group,[14,15,16] and f-block metal complexes.[17,18] As a specific example, the Heyduk group has reported complexes using d^0 metals such as tantalum (V) and zirconium (IV) that incorporate redox-active pincer-type ligands.[19] The group focused on the bis(2-isopropylamino-4-methoxyphenylamine) (NNN) ligand, which has the ability to exist across a series of three oxidation states (Figure 1).

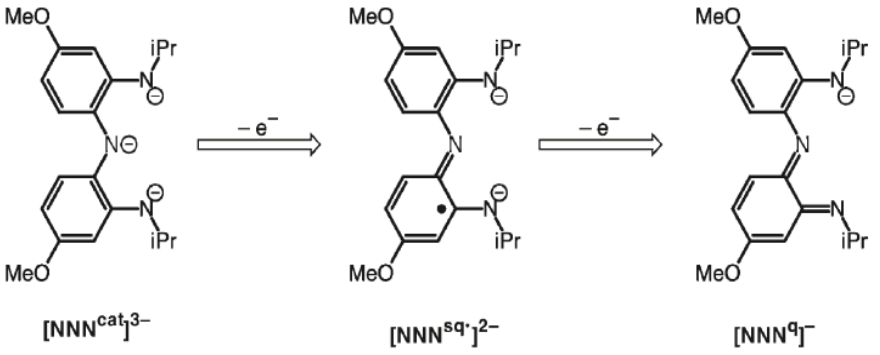

Figure 1: The three common oxidation states of the ligand platform [NNN] utilized by Heyduk et al. Reproduced from Heyduk et al.[19]

In its fully reduced state, the [NNN] ligand is in the catecholate ($[NNN^{cat}]^{3-}$) form. Removal of one electron affords the semiquinonate state ($[NNN^{sq}]^{2-}$), and finally, the removal of the second electron results in the quinonate form of the ligand ($[NNN^{q}]^{-}$). Heyduk and co-workers then used the pincer ligand to synthesize tantalum and zirconium

complexes, the latter of which is shown in Figure 2. The redox-active ligands play an essential role in the chemistry performed by the Heyduk group, as the metal-ligand molecular orbitals promote reaction chemistry while the metal center maintains a constant d^0 configuration.

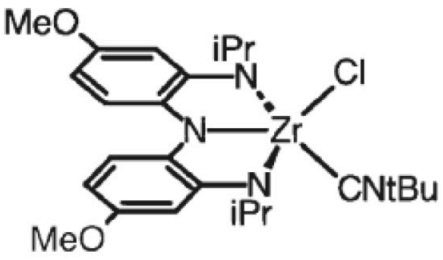

Figure 2: [NNN^{cat}]ZrCl(CN*t*Bu) synthesized by Heyduk et al. Reproduced from from Heyduk et al.[19]

For example, the group developed catalytic chemistry around the complex that features a pincer ligand, zirconium center, and isocyanide (CN*t*Bu) ligand, for a nitrene transfer reaction (Scheme 1). The redox activity of the ligands promotes reaction and the zirconium center remains at a constant oxidation state in a d^0 configuration to produce the desired carbodiimide (*t*BuN=C=NR) product. The use of the complex in such a reaction provides an example of how the use of redox-active ligands can enable new reactivity for d^0 metals, that would otherwise be unattainable.

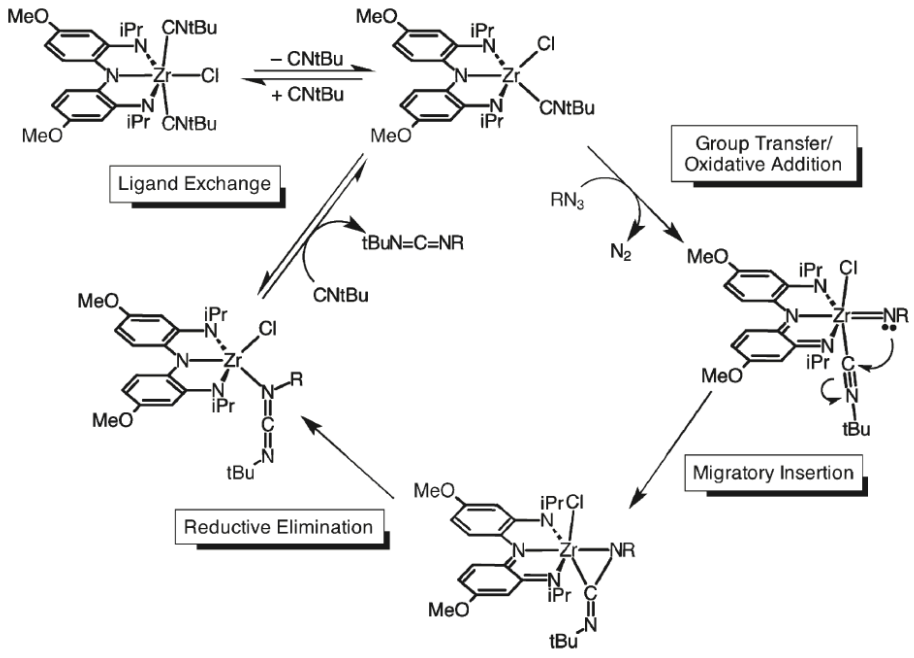

Scheme 1: Simplified mechanism for the nitrene-transfer reaction using [NNN^{cat}]ZrCl(CN*t*Bu). Reproduced from Heyduk et al.[19]

In a similar manner, redox-active ligands can also be applied to an aluminum framework. The use of such redox-active ligands around an Al(III) ion would result in aluminum coordination complexes that could exist over a range of oxidation states, making available new reaction pathways that could be exploited to expand the utility of aluminum-based catalysts. Seminal work from the Berben group has applied this concept using iminopyridine ligands, specifically using 2,6-bis(1-methylethyl)-*N*-(2-pyridinylmethylene)phenylamine, (IP).[14] The group synthesized a variety of aluminum complexes of the form (IP^{n-})Al-X, in a wide range of oxidation states including: $(IP^{0})AlCl_3$, $(IP^{1-})_2AlCl$, and $[(DME)_3Na][(IP^{2-})_2Al]$ (Figure 3a). The group used electrochemistry to probe the redox behavior of the compounds. For instance, $(IP^{-})_2AlCl$ has two successive one-electron oxidation events that correspond to the $IP^{0/1-}$ couples of the two ligands (Figure 3b). Thus, the Berben group demonstrated that redox-active ligands could be employed in order to impact a rich redox activity to aluminum complexes.

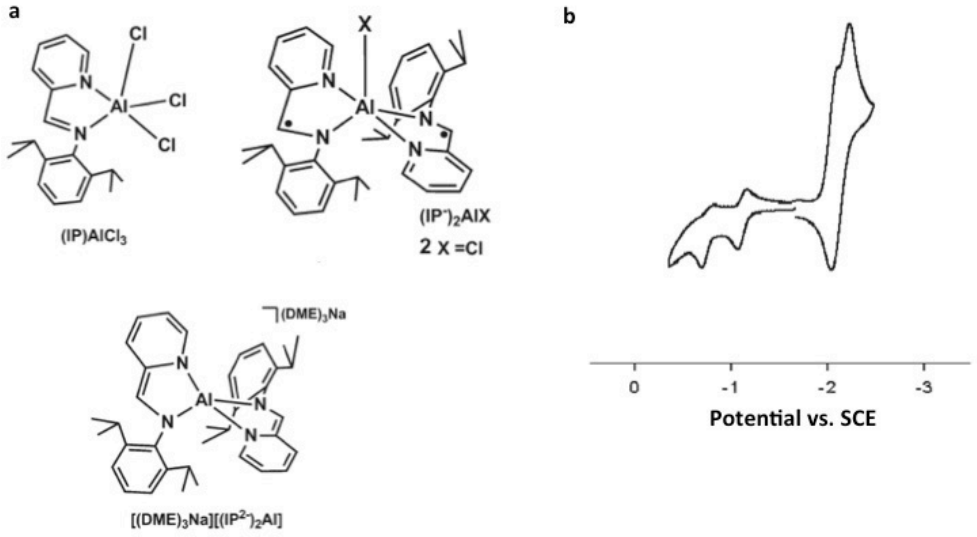

Figure 3: (A) Aluminum complexes $(IP^{0})AlCl_3$, $(IP^{-})_2AlCl$, and $[(DME)_3Na][IP^{2-})_2Al]$ synthesized by Berben et al. (B) Cyclic voltammogram for a 1mM solution of $(IP^{-})_2AlCl$ recorded in 0.3 M Bu_4NClO_4 THF solution. Reproduced from Berben et al.[14]

In addition to using ligands to transfer electrons, researchers have also expanded the reactivity of elements through chemically non-innocent or cooperative ligands, which utilize intramolecular cooperation.[20] Metal-ligand cooperation has become an important concept in catalysis in which both the metal and ligand are directly involved in bond activation processes (Scheme 2).[21]

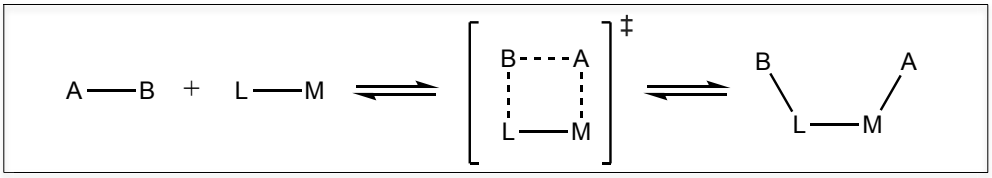

Scheme 2: Bond activation by metal-ligand cooperation. Where L represents a ligand, M and metal, and A and B represent an arbitrary compound. Modified from Berben et al.[20]

Similar to the use of redox non-innocent ligands, numerous researchers have used cooperative ligands to expand the reactivity of a variety of elements. For example, Gelman et al. reported an iridium pincer complex that utilized metal-ligand cooperation to catalyze the acceptorless dehydrogenation of alcohols.[22] The group synthesized a new bifunctional dibenzobarrelene-based $PC_{sp3}P$ pincer ligand (Figure 4 left). In order to probe the ability of the complex to incorporate different functional groups, the Gelman group designed an iridium hydride pincer complex with an acidic side arm (Figure 4 right).

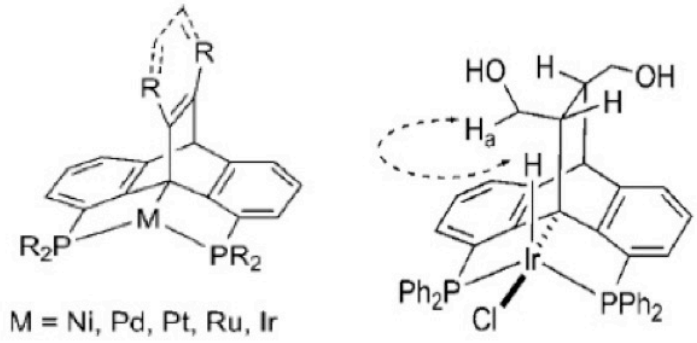

Figure 4: Left: general structure of the metalated C_{sp3} pincer compounds designed by Gelman et al. 2011. Right: Iridium hydride pincer complex designed by Gelman and co-workers. Reproduced by Gelman et al. 2011.[22]

In an attempt to crystallize the structure, researchers discovered that the compound transforms into a new complex devoid of hydride signals in the ^1H NMR

spectrum. The group proposed a hypothetical catalytic cycle in which the acceptorless dehydrogenation of alcohols could proceed (Scheme 3). The mechanism involves the formation of an iridium-oxygen bond and a ligand exchange step. The group then tested the reactivity of their compound. The oxidation of 1-phenylethanol under acid or base free conditions in the presence of 0.1 mol% of the iridium hydride pincer compound resulted in the desired acetophenone.[22] Thus, Gelman et al. proposed a mechanism for the dehydrogenation of alcohols that involved intramolecular cooperation between the functionality and the metal center of their newly synthesized iridium complex.[22]

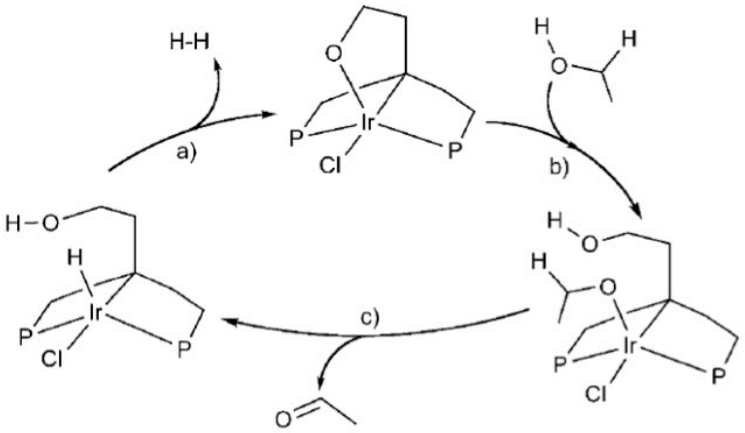

Scheme 3: Proposed mechanism by Gelman et al. for the dehydrogenation of alcohols by an iridium hydride pincer complex.[22]

In a similar manner, the Berben group reported the activation of N-H bonds by a molecular aluminum complex via metal-ligand cooperation. The group used a tridentate bis(imino)pyridine ligand ($^{Ph}HI_2P^-$) to synthesize both the tetrahydrofuran (THF) adduct and a base free aluminum hydride complex, ($^{Ph}HI_2P^{2-}$)AlH(THF), and ($^{Ph}HI_2P^{2-}$)AlH (Figure 5).[23] Using the base free complex, the group added H_2NDipp (dipp – 2,6-diisopropylphenyl) to form ($^{Ph}HI_2P^-$)AlH(NHDipp) which results from addition of the N-H bond across the aluminum-amido bond (Scheme 4). The group expanded this chemistry to investigate the ability of the compound to perform as a catalyst for amine dehydrogenation. In this vein, they added

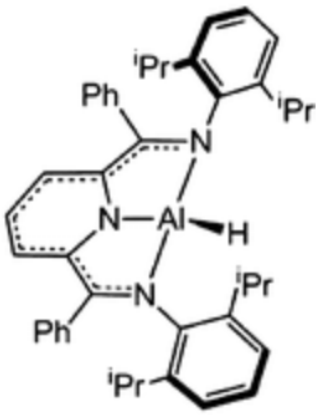

Figure 5: Structure of ($^{Ph}HI_2P^{2-}$)AlH synthesized by Berben et al. Reproduced from Berben et al. [23]

benzylamine with 20 mol% catalyst loading of ($^{Ph}HI_2P^{2-}$)AlH. The formation of *N*-(phenylmethylene)benzene-methanamine was observed with 75% conversion and 3.6 catalytic turnovers. Thus, the Berben group demonstrated that the bis(imino)pyridine complex of aluminum can activate N–H bonds via metal-ligand cooperation and that the compound can be used to catalyze amine dehydrogenation.[23]

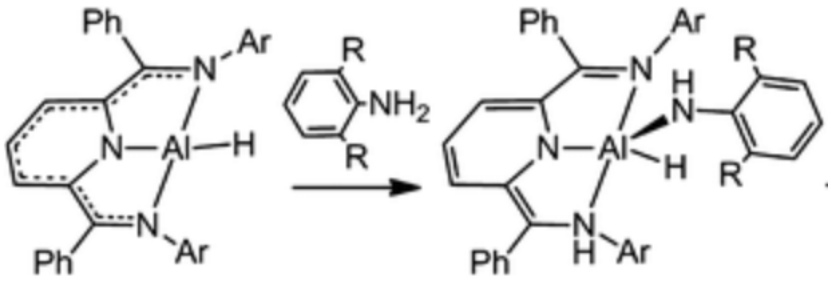

Scheme 4: Addition of H_2NDipp to ($^{Ph}HI_2P^{2-}$)AlH and the resulting product. Reproduced from Berben et al.[23]

Research in the Graves group has focused on the development of novel aluminum complexes for application in catalysis. The group has a specific interest in the synthesis of aluminum complexes of redox-active ligands across various activation states as well as ligands that promote metal-ligand cooperative reaction pathways. An understanding of the electronic structure and fundamental reactivity patterns of the compounds guides the development of such catalytic complexes. My efforts in this area have focused on the preparation of aluminum coordination complexes implementing ligands containing nitroxide functional groups. The nitroxide functional group is known to exist over three oxidation states (Figure 6). The states include the fully reduced form of the nitroxide group ($R_2N\text{-}O^-$), the neutral radical form ($R_2N\text{-}O\bullet$), and the fully oxidized oxoammonium cation ($R_2N{=}O^+$).

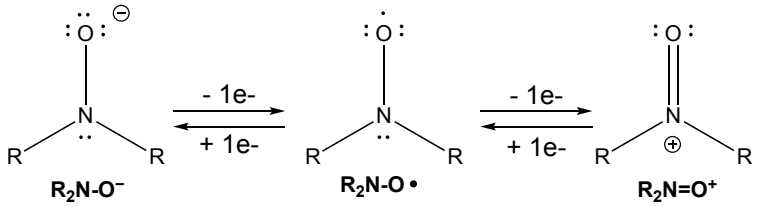

Figure 6: The NO functional group across thee oxidation states.

The Graves group has previously prepared complexes of pyridyl hydroxyl amines of the form: $(^{R}pyNO^{-})_2AlCl$ where $(^{R}pyNO^{-})$ = *N*-*tert*-butyl-*N*-(2-(5-R-pyridyl))nitroxyl, R = H, CH_3, CF_3 and explored their electrochemical behaviour (Figure 7).[24]

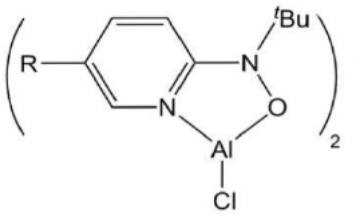

Figure 7: Structure of $(^{R}pyNO^{-})_2AlCl$ synthesized by Poitras et al. where R = H, CH_3, or CF_3. Reproduced from Poitras et al.[24]

They demonstrated that pyridyl nitroxide ligands could be coordinated to an Al(III) ion, generating a new class of aluminium compounds supporting redox-active ligands. Electrochemical characterization of these compounds displayed two redox events and the group showed that the oxidation potentials of the redox events could be tuned through ligand substituents with more electron donating groups resulting in the most negative potentials and electron withdrawing groups the most positive potentials. However, the $(^{R}pyNO^{-})_2Al$ complexes showed poor electrochemical reversibility, indicating decomposition on an electrochemical timescale. Also, they were unable to chemically oxidize the complexes, resulting in unreacted starting material or free ligand, depending on the strength of the oxidant. As a continuation of the work previously completed by the Graves lab,[24,25] I sought to develop a more robust Al-nitroxide compound implementing a tripodal nitroxide ligand: $[\{(2^{t}BuNO)C_6H_4CH_2\}_3N]^{3-}$ ($TriNOx^{3-}$).[26] $TriNOx^{3-}$ has a greater number of bonding sites, which should increase the chelate effect as compared to the pyridyl hydroxyl amine

system. Additionally, throughout the redox chemistry of the ($TriNOx^{3-}$)Al complex, the ligand should maintain some alkoxide character across oxidation states, which we hypothesized would increase the stability of the complex and result in a ligand that stays bound to the metal ion upon reaction. Therefore, implementing the tetradentate ligand should provide a more robust complex with better electrochemical reversibility that also stays intact during chemical oxidation and could thus be explored as a catalyst for redox reactions.

In this thesis, I will report the preparation and characterization of the aluminium complex of the tripodal nitroxide ligand ($TriNOx^{3-}$)[26] as well as its gallium and indium analogs. Expanding the synthetic chemistry developed through the preparation of the aluminum complex to the other Group 13 metals results in a suite of nitroxide-based ligand complexes that vary in electronic parameters, steric profiles, and metal ionic radius and can be tuned to different reactions. I will also demonstrate the accessible redox chemistry of the newly synthesized aluminum complex through one-electron oxidations. The one-electron oxidations help support the hypothesis that the redox chemistry of ($TriNOx^{3-}$) can be coupled with reaction chemistry. In addition, I will outline the catalytic activity of the ($TriNOx^{3-}$)Al complex toward carbonyl hydroboration utilizing metal-ligand cooperation. Hydrofunctionalization reactions are a common route to build complex organic molecules from readily available starting materials and systems utilizing metals across the periodic table have been reported.[27,28,29] The use of our aluminum complex in an important organic reaction demonstrates new activation parameters that result in transition-metal-like catalysis.

2. Results and Discussion

2.1 Synthesis and characterization of a tripodal tris(nitroxide) aluminum complex: (TriNOx^{3-})Al-py

First and foremost, (TriNOx)H_3 was synthesized as described by the Schelter group.[26] The ligand can be synthesized using a lithium-halogen exchange reaction between tris-2-bromobenzylamine and ^{n}BuLi at –78°C, followed by the addition of 2-methyl-2-nitrosopropane dimer (Scheme 5). The reaction is then quenched using aqueous NH_4Cl solution. After separating the layers, the organic layer is collected and dried. After the drying agent is removed by filtration, volatiles are removed under reduced pressure, yielding crude material. The crude mixture is purified by recrystallization from a boiling mixture of hexane and dichloromethane, yielding pure (TriNOx)H_3. I routinely run this reaction on a gram-scale and isolate pure ligand in 57% yield.

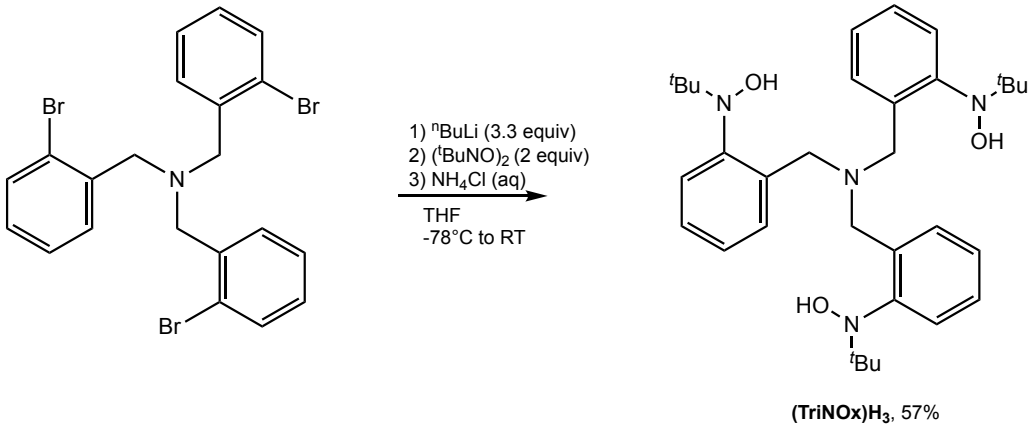

Scheme 5: Synthesis of (TriNOx)H_3 ligand, as prepared by Schelter et al.[26]

Reaction of (TriNOx)H_3 with three equivalents of $NaN(SiMe_3)_2$ results in a deprotonated compound which can then be followed by salt metathesis with $AlCl_3$. The reaction mixture is then filtered over Celite and washed with THF to remove the NaCl salt byproduct. After volatiles are removed, the mixture is stirred in pyridine in order to

coordinate a pyridine to the cleft of the aluminum, which creates a more easily isolable product as it begins to crystallize. Next, volatiles are removed and the compound taken up into toluene to remove any remaining salts and $HN(SiMe_3)_2$ is removed under vacuum. After solvents are removed (TriNOx^{3-})Al-py (**1**) can be isolated as a tan solid. This reaction is regularly run on a gram scale and the compound is isolated in 77% yield (Scheme 6).

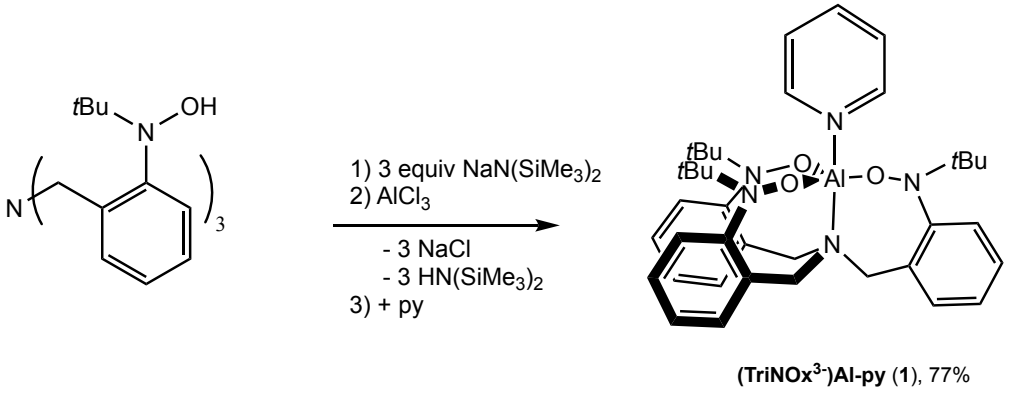

Scheme 6: Synthesis of the (TriNOx^{3-})Al-py (**1**) complex by salt metathesis.

Complex **1** was readily characterized by ^{1}H NMR and ^{13}C NMR spectroscopy. The ^{1}H NMR spectrum exhibits a single upfield (1.44 ppm) resonance that integrates to 27 hydrogens and can be assigned to the *t*Bu groups. The single signal designates 3-fold symmetry of the tripodal ligand when bound to the metal center. In addition, the spectrum displays two doublets (J=11.2 Hz) corresponding to diastereotopic hydrogens of the bridgehead CH_2 group. Each resonance integrates to three protons. The aromatic region has a variety of peaks consisting of a series of four multiplets that integrate to three protons. The resolution of the aromatic region not only demonstrates the four individual hydrogens on the phenyl ring present in the ligand, but also further indicates 3-fold symmetry. Resonances corresponding to pyridine can also be seen in the aromatic region (8.57 ppm, 6.97 ppm, 6.64 ppm), providing further evidence for the presence of the group

in the cleft of the aluminum center. The ^{13}C NMR spectrum displays resonances corresponding to the *t*Bu groups, methylene carbons, and six unique aromatic carbons in addition to the three carbons corresponding to the pyridine. Single crystals of complex **1** were grown from a concentrated pyridine solution at –25°C, which allowed X-ray crystallography to confirm the formulation of (TriNOx^{3-})Al-py (Figure 8). As shown, the aluminum ion is penta-coordinate with a distorted trigonal bipyramidal geometry (τ_5 = 0.88).[30] The (TriNOx^{3-}) ligand is disordered, with the two contributing structures being mirror images of each other. The average N–O distance in compound **1** is 1.44 Å, which compares well with analogous parameters for the series of rare earth (TriNOx)RE complexes prepared by the Schelter group ($N–O_{ave}$ = 1.44 Å)[31] and suggests a fully reduced ligand in complex (**1**).

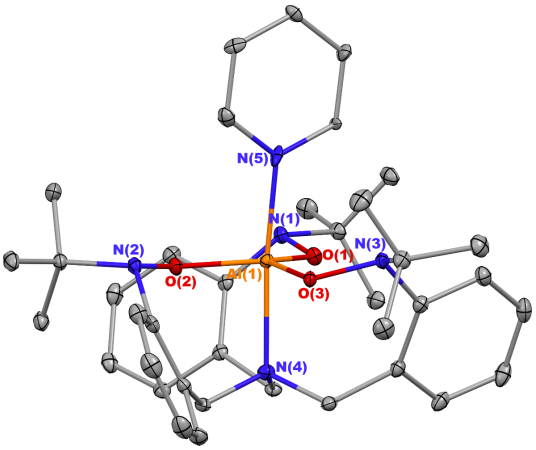

Figure 8: Solid state structure of (TriNOx^{3-})Al-py complex. Ellipsoids are projected at 50% probability hydrogen atoms are omitted for clarity.

As discussed above, the nitroxide functional group can exist across three oxidation states. As hypothesized, the redox capabilities of the TriNOx^{3-} ligand are retained during complexation to the Al(III) center and compound **1** has the ability to exist over a series of oxidation states. The cyclic voltammogram of compound **1** (Figure 9) exhibits two reversible features, correlating to the sequential one-electron oxidation processes of the ligand to form [(TriNOx^{2-})Al-py]$^{+}$ and [(TriNOx^{1-})Al-py]$^{+}$. Mackinsey Smith performed density functional theory calculations of singly and doubly oxidized

products to support this assignment. More details can be found in Mackinsey Smith's thesis. The electrochemistry supports the hypothesis that the multidentate nitroxide complexes can be used to impart a rich redox activity to the aluminum complex. Moreover, the current system provides reversible redox events as compared to the irreversible activity seen for the (^{R}pyNO^{-})$_2$AlCl complexes. The reversible peaks not only indicate the successful synthesis of a redox-active aluminum compound, but also that the compounds are stable on an electrochemical timescale. Therefore, the goals of improving electrochemical reversibility and stability were reached using the (TriNOx)H_3 ligand.

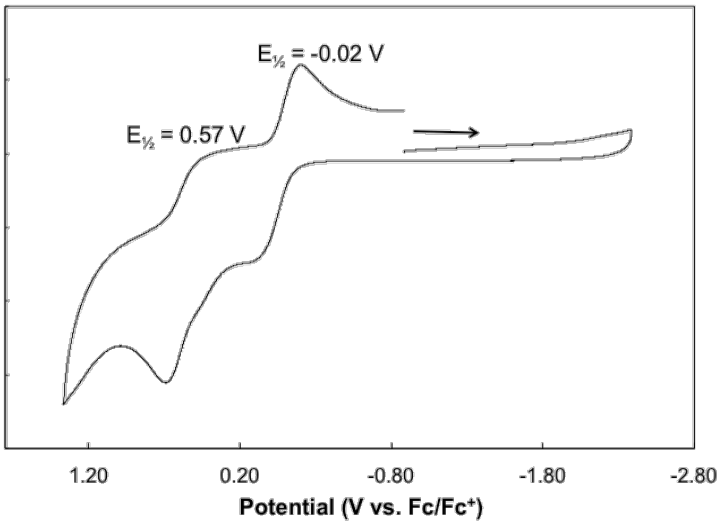

Figure 9: Cyclic voltammogram of (TriNOx^{3-})Al-py recorded in 0.1 M [*n*-Pr$_4$N][BAr$_F$] THF solution recorded at 500 mV/s.

2.2 Synthesis and characterization of tripodal tris(nitroxide) gallium and indium complexes: (TriNOx^{3-})Ga and (TriNOx^{3-})In

In light of the successful synthesis of (TriNOX^{3-})Al-py, we sought to expand the use of the TriNOx^{3-} ligand to other group 13 metals, specifically gallium and indium. The creation of such compounds would provide a suite of nitroxide-based ligand complexes that vary in electronic parameters, steric profiles, and metal ionic radius, allowing for the substitution of the metal center to be tuned to different reactions. In a similar manner to compound **1,** reaction of (TriNOx)H_3 with 3.4 equivalents of NaN(SiMe$_3$)$_2$ results in a deprotonated compound which can then be followed by salt metathesis with $GaCl_3$. The

solution is then filtered over Celite and washed with THF to remove the NaCl byproduct. After volatiles are removed the mixture was stirred in pyridine in order to explore if a pyridine would attach to the cleft of the gallium as was seen in the aluminum counterpart. Next, volatiles are removed and the compound was taken up into dichloromethane to remove any remaining salts. (TriNOx^{3-})Ga (**2**) can be isolated as a tan solid in a 79% yield (Scheme 7).

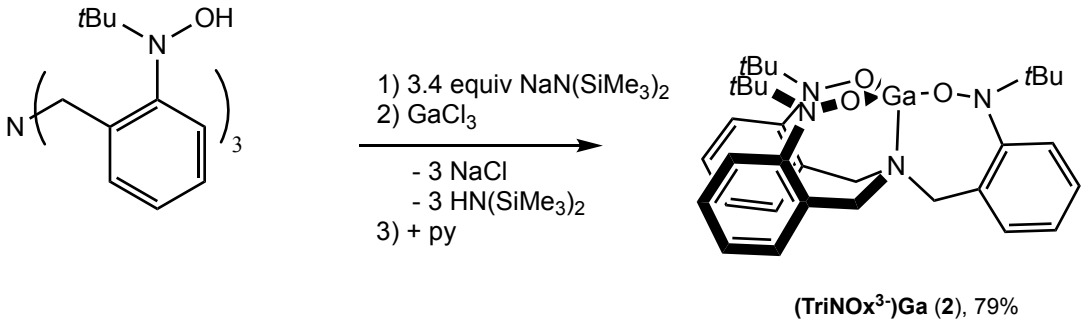

Scheme 7: Synthesis of (TriNOx^{3-})Ga (**2**) by salt metathesis.

Complex **2** was readily characterized by ^{1}H NMR and ^{13}C NMR spectroscopy, with the spectra for **2** being similar to that for compound **1**. The ^{1}H NMR spectrum displays a single resonance at 1.41 ppm that integrates to 27 hydrogens and can be assigned to the *t*Bu groups, the protons of the bridgehead CH_2 groups are diastereotopic, resulting in two doublets (J=11.4 Hz), which integrate to three protons each. The aromatic region illustrates four multiplets that integrate to three protons each, demonstrating the four hydrogens on the aromatic ring of the ligand arm. Together, this supports a fully

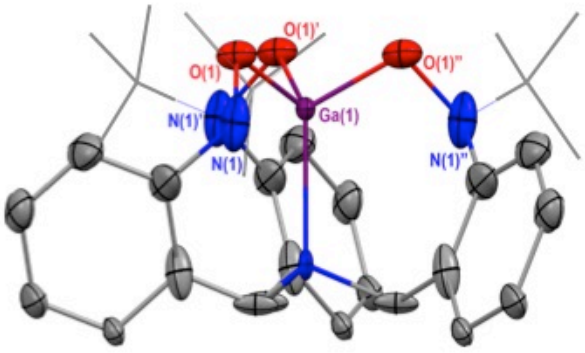

Figure 10: Solid state structures of (TriNOx^{3-})Ga. Ellipsoids are projected at 50% probability and hydrogen atoms are omitted for clarity. *tert*-Butyl groups are depicted using a wireframe model.

coordinated TriNOx^{3-} ligand, resulting in a 3-fold symmetric gallium complex. Contrary to compound **1**, (TriNOx^{3-})Ga does not have a pyridine coordinated in the cleft as neither the ^{1}H NMR nor ^{13}C NMR show any peaks corresponding to a pyridine. The ^{13}C NMR spectrum displays resonances corresponding to the *t*Bu groups, methylene carbons, and six unique aromatic carbons. Single crystals of complex **2** were grown from a layered THF and hexane solution at –25°C, which allowed X-ray crystallography to confirm the formulation of (TriNOx^{3-})Ga, also providing further evidence for the lack of pyridine coordinated to the metal (Figure 10). One proposed reason for the lack of pyridine is that the Ga^{3+} ion is less Lewis acidic than the Al^{3+} metal center.[32] Therefore, comparisons regarding bonding lengths between the gallium and aluminum complexes would not be informative because the two complexes are not completely analogous.

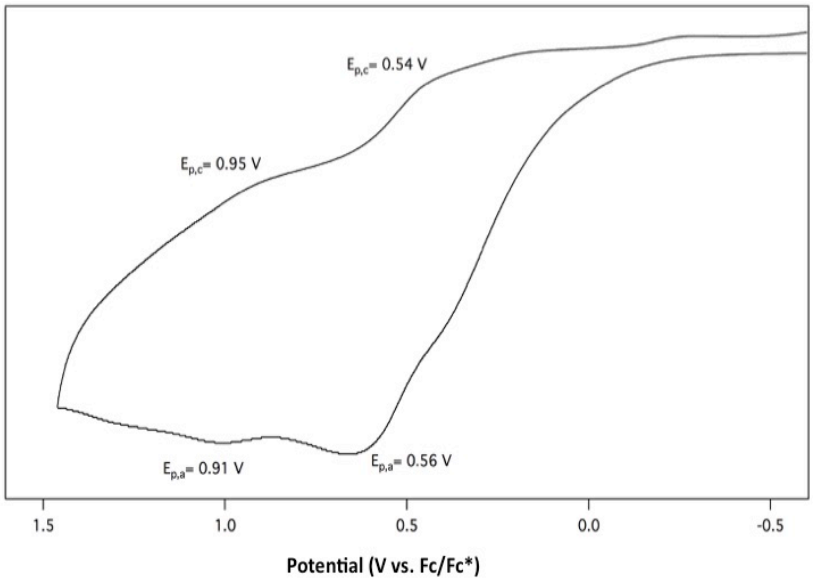

Figure 11: Cyclic voltammogram of (TriNOx^{3-})Ga recorded in 0.1 M [*n*-Pr_4N][BAr_F] MeCN solution, recorded at 500 mV/s.

In a similar manner to complex **1**, it was hypothesized that the redox capabilities of the nitroxide ligand would be conserved when bound to the gallium center. We again tested this theory using electrochemistry. The cyclic voltammogram of (TriNOx^{3-})Ga was collected in MeCN (as compared to THF used for compound **1**) and illustrates two non-reversible redox events corresponding

to the sequential one-electron oxidation processes of the ligand to form $[(TriNOx^{2-})Ga]^{+}$ and $[(TriNOx^{1-})Ga]^{2+}$ (Figure 11). The electrochemistry confirms that the gallium compound (**2**) is redox-active. The redox processes of compound **2** are non-reversible, compared to the reversible processes seen for $(TriNOx^{3-})$Al-py (**1**). As with the crystal structure, comparison of the redox potentials between complex **1** and compound **2** are not highly informative due absence of the pyridine in the gallium structure and because the experiments were run in different solvents. Electrochemistry of compound **2** was also run in THF, but performing the experiment in MeCN gave better results. However, one non-reversible redox event can be seen at in THF with an $E_{p,a}$ value of 0.50 V and $E_{p,c}$ value of 0.49 V (both referenced to ferrocene), similar to the results of the first redox process in acetonitrile. Nonetheless, the open cleft does support the shift of redox events to more positive potentials relative to those observed for $(TriNOx^{3-})$Al-py. Despite the differences in structure compared to $(TriNOx^{3-})$Al-py, it is clear that we have successfully synthesized a redox-active gallium complex utilizing a multidentate nitroxide-based ligand.

Continuing down the periodic table, our next goal was to synthesize an indium compound using the same $(TriNOx)H_3$ ligand. Although the syntheses of compound **1** and **2** were very similar, it is hypothesized that the solubility of $(TriNOx^{3-})$In (**3**) caused prepared material to be lost in purification steps. $(TriNOx^{3-})$In is only sparingly soluble in THF, and is significantly less soluble than the aluminum or gallium analogs. Thus, after the initial salt metathesis any purification steps removed the product from solution and a modified synthetic procedure was developed.

$[In(NEt_2)_3]_2$ was reacted with two equivalents of $(TriNOx)H_3$ in toluene. After stirring for 12 hours pyridine was added to the solution. After the removal of filtrates, the reaction is taken back up into pyridine and stored at –25°C. $(TriNOx^{3-})$In (**3**) precipitates from solution and can be isolated as a white solid in 57% yield (Scheme 8).

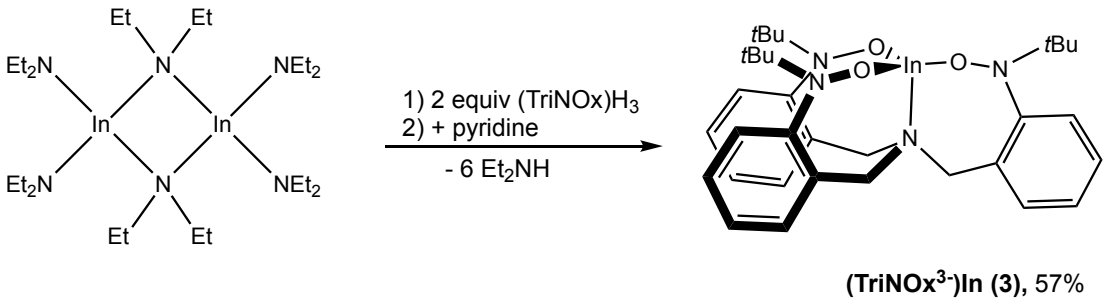

Scheme 8: Synthesis of $(TriNOx^{3-})$In (**3**).

The indium diethylamine serves as both the base and the source of indium. The diethylamide groups are basic and deprotonate the hydroxyl group on the ligand to install the In-O bonds. The use of the indium dimer as both a Lewis base and source of indium encourages the complexation of the metal to the ligand. A major advantage of this route is that the only byproduct formed is $HNEt_2$, which can be easily removed under vacuum and facilitates the purification of the $(TriNOx^{3-})$In complex.

Again, the compound was characterized by ^1H NMR and ^{13}C NMR spectroscopy. Analogous to compounds **1** and **2** a single resonance at 0.99 ppm integrates to 27 hydrogens and can be assigned to the *t*Bu groups, which also suggests 3-fold symmetry of the ligand when bound to the indium center. As seen in compounds **1** and **2**, the spectrum includes two doublets (J = 10.8 Hz), which integrate to three protons that correspond to the diastereotopic hydrogens of the CH_2 group on the bridgehead. The aromatic region displays four multiplets that integrate to three protons each, corresponding to four unique aromatic hydrogens and further confirming 3-fold

symmetry. It is also important to note that the ^{1}H NMR experiment was run in pyr-d_5 and thus this method of characterization could not be used to confirm the presence or absence of a pyridine in the cleft of the metal. Similar to complexes **1** and **2**, the ^{13}C NMR spectrum displays resonances corresponding to the *t*Bu groups, methylene carbons, and six unique aromatic carbons. The compound was also characterized via elemental analysis. Theoretically, (TriNOx^{3-})In should be 60.00% carbon, 6.87% hydrogen, and 8.48% nitrogen. It was found that complex **7** was 59.67% carbon, 6.70% hydrogen, and 8.27% nitrogen, all of which fall within a 0.33% deviation from the theoretical values. The results confirm both the successful synthesis of the compound and absence of pyridine in the cleft, which could be due to the decrease in Lewis acidity of In^{3+} compared to Al^{3+}.

Whereas electrochemistry was used to visualize the redox processes of the gallium and aluminum complexes, the low solubility of compound **3** prevented the collection of such data. The compound does not produce a homogeneous solution in MeCN, THF, DCM, or a variety of other solvents, and performing electrochemistry in pyridine is not possible. Thus, in order to test whether the redox ability of the ligand correspond to the indium complex, as shown for the aluminum and gallium, other avenues will need to be explored.

2.3 Oxidation chemistry of (TriNOx^{3-})Al-py

After demonstrating the redox capabilities of (TriNOx^{3-})Al-py (**1**) using electrochemistry, we sought to chemically oxidize the complex, thus coupling redox

chemistry to chemical activity. In that vein, we reacted complex **1** with a series of one-electron oxidants including XeF_2, [Fc][BPh_4], and CuCl.

Reaction of compound **1** with one equivalent of XeF_2 results in the formation of ($TriNOx^{2-}$)Al-F (**4**) in a 77% yield. The complex is NMR silent. Similarly, the oxidation of complex **1** was successful with ferrocenium (Fc^+). Reaction of ($TriNOx^{3-}$)Al-py with one equivalent of [Fc][BPh_4] generated an equivalent of ferrocene and [($TriNOx^{2-}$)Al][BPh_4] (**5**) in a 58% yield. As with **4**, compound **5** does not exhibit signals in the NMR spectrum, again indicating a paramagnetic compound. Along the same lines, the reaction of ($TriNOx^{3-}$)Al-py with 1.7 equivalents of CuCl generates ($TriNOx^{2-}$)Al-Cl (**6**) l in a 51% yield. As with compounds **4** and **5**, complex **6** is NMR silent also suggesting a paramagnetic complex. Compounds **4** and **5** were also characterized via elemental analysis (details are in the Methods and Materials). While crystal structures of the oxidation products have been elusive, Figure 12 provides predicted structures of compounds **4-6**. As seen in Figure 12, the oxidation of complex **1** using halide transfer agents is commensurate with the installation of an Al–X (X = F, Cl) bond. However, the successful oxidation of the compound using [Fc][BPh_4] indicates that the installation of a new bond at the aluminum center is not necessary for oxidation.

Based off of the lack of resonances seen in the ^1H NMR spectra, Mackinsey Smith performed electron paramagnetic resonance spectroscopy (EPR) on compounds **4, 5,** and **6** in order to confirm the presence of and visualize the position of the radical. The spectra of all three oxidized materials are similar and support a radical localized on one nitroxide arm of the ligand. More details on these experiments can be found in Mackinsey Smith's thesis.

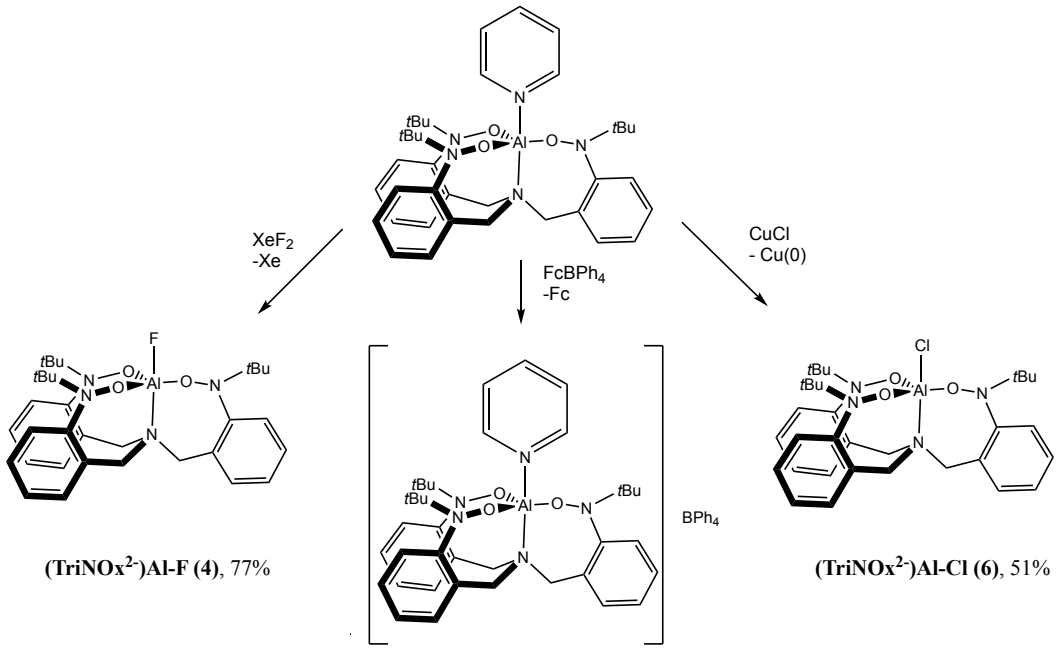

Figure 12: Proposed products of one-electron oxidations of ($TriNOx^{3-}$)Al-py.

The successful oxidation of ($TriNOx^{3-}$)Al-py demonstrates that the use of the more robust ligand serves its hypothesized function. As compared to the pyridyl hydroxyl amine system, neither free ligand nor unreacted starting materials are detected in the oxidation reactions of complex **1**. Overall, through the use of one-electron oxidants, we were able to couple the chemistry of the first redox event seen in the cyclic voltammogram to chemical reactivity. In the future, it would be fruitful to pursue two-electron oxidants and couple both redox events seen in the electrochemistry to redox chemistry, using oxidizing agents such as $PhICl_2$.[33]

Additionally, such experiments can be expanded to compounds **2** and **3**. We have begun chemical oxidation experiments using the gallium complex, and utilization of such methods would also help confirm the redox activity of the indium compound.

2.4 Hydroboration of Carbonyls using (TriNOx^{3-})Al-py as a catalyst

After synthesizing an aluminum redox-active complex and investigating the ability of such a compound to participate in oxidation reactions, we looked to implement the complex as a catalyst in organic reactions.

It is important to note that (TriNOx^{3-})Al-py has both Lewis acidic and Lewis basic character. The Lewis acidity comes from the Al^{3+} metal center, whereas the Lewis basicity is found through the nitroxide nitrogens on the ligand arms. The Lewis acidity was gauged by its measured acceptor number (AN) value of 75.[34,35,36] For reference, some common acceptor numbers are: hexane, 0; water, 55; boron trichloride, 97, and trifluoroacetic acid, 105; thus higher acceptor numbers correspond to more Lewis acidic compounds.[37] The compound is clearly Lewis acidic and also has basic character through the nitrogen atoms on the ligand arms.

With this in mind, the dual nature of compound **1** opens the possibility for metal-ligand cooperative bifunctional catalysis. The application of aluminum complexes as catalysts for the reduction of organic substrates has gained traction in recent years,[38,39] including systems for the hydroboration of carbonyls. Thus, we began our exploration of using (TriNOx^{3-})Al-py as a catalyst in the hydroborations of ketones, specifically with pinacolborane (HBpin).

Using 10 mol% loading of complex **1** and 1.2 equivalents of HBpin the reduction of acetophenone was accomplished in a 54% yield after 20 hours at room temperature. Performing the reaction under the same conditions and time frame at 75°C resulted in a 75% yield. The activity of the catalyst was dramatically improved with the removal of the pyridine: using 10 mol% (TriNOx^{3-})Al (**7)** and 1.2 equivalents of HBpin results in

hydroboration of acetophenone to give the borate ester **i** in quantitative yield (NMR yield) in 20 hours at room temperature (Scheme 9). When the analogous reaction was run without catalyst under the same conditions no product was formed. These optimized conditions were applicable to a wide range of ketones (Scheme 9). Interestingly, both electron-withdrawing and electron-donating groups significantly reduced the yield of borate ester product **ii** and **iii**. The reduction of benzophenone was more difficult, resulting in the reduced product in an 18% yield. The yield was greatly improved to 53% when heated to 75°C. The reduction of benzylideneacetone at room temperature generated product **v** in a 60% yield, and in this case heating the reaction to 75°C resulted in a lower yield. It is hypothesized that the lower yield results from competitive reactivity with the alkene. Finally, the reduction of aliphatic ketones was also successful, with the reduction of both 2-octanone and cyclohexane producing greater than a 90% yield.

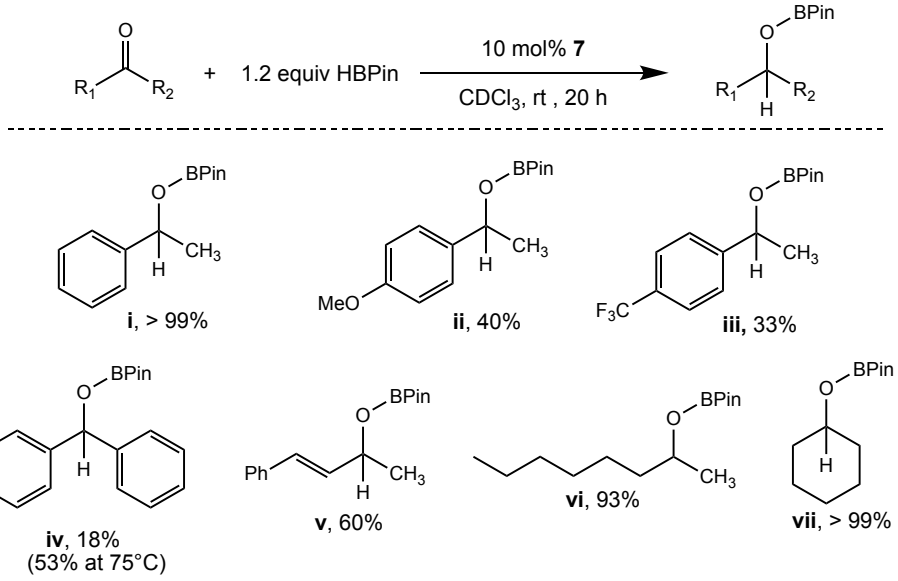

Scheme 9: Scope of hydroboration of ketone substrates. Reaction conditions: Ketone (0.5 mmol), HBpin (0.6 mmol), (TriNOx^{3-})Al (0.05 mmol), $CDCl_3$ (1.0 mL). Yields were determined by ^1H NMR spectroscopy using hexamethylcyclotrisiloxane (0.083 mmol) as an internal standard.

The hydroboration protocol could also be extended to aldehydes. As expected, the aldehyde substrates are more easily reduced compared to their ketone counterparts due to steric and electronic effects.[40] Therefore, high yields could be obtained using only 5 mol% catalyst loading of compound **7** in four hours at room temperature (Scheme 10). In contrast to the ketone system, both electron-donating (**ix**) and electron-withdrawing (**x**) substituents were tolerated without a significant decrease in yield. The system was applicable to both aromatic and aliphatic aldehydes.

In comparison to other aluminum catalytic systems used toward the hydroboration of carbonyls, (TriNOx^{3-})Al is less active and higher catalyst loads are required to obtain similar yields.[38,39] One explanation for the difference could be attributed to the suggested mechanism. Previous systems implement compounds that have an Al-H moiety, which is proposed to insert into the carbonyl in a key mechanistic step. On the other hand, (TriNOX^{3-})Al does not have an Al-H and it is thought that the catalyzed hydroboration of aldehydes and ketones operates through metal-ligand bifunctional catalysis (Scheme 11).

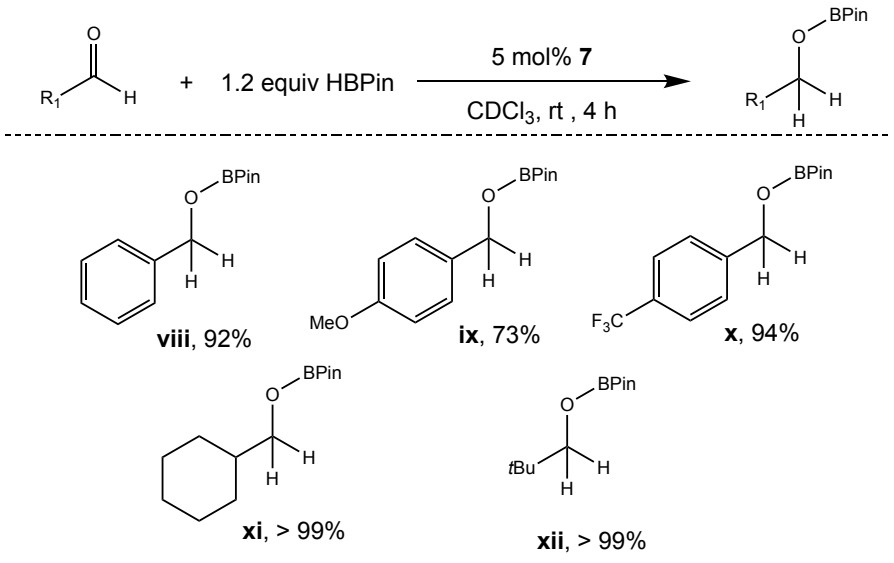

Scheme 10: Scope of hydroboration of aldehyde substrates. Reaction conditions: Ketone (0.5 mmol), HBpin (0.6 mmol), (TriNOx^{3-})Al (0.025 mmol), $CDCl_3$ (1.0 mL). Yields were determined by ^{1}H NMR spectroscopy using hexamethylcyclotrisiloxane (0.083 mmol) as an internal standard.

In the proposed mechanism the aluminum metal can bind to the carbonyl while the borane simultaneously coordinates to one of the nitroxide nitrogens of the ligand. The borane bond creates an adduct that polarizes the B-H bond toward hydrogen and thus increases its hydricity. Similar activation was reported in the NaOH-catalyzed hydroboration system developed by Wu et al[41] and the mechanism closely resembles the Corey-Bakshi-Shibata reduction mechanism.[42] Largely, the dual activation results in the delivery of the hydride to the carbonyl with installation of the B-O bond to turn over the catalyst.

The proposed mechanism is supported by numerous factors. First, the removal of the pyridine from complex **1**, resulting in compound **7**, produces the desired product in higher yields at room temperature. The removal of the pyridine allows the cleft of the aluminum ion to remain open, permitting faster binding and thus higher yields, indicating that the aluminum ion participates in some form of bonding throughout the reaction. Second, the ^{11}B NMR spectrum of a mixture of HBpin and (TriNOX^{3-})Al, shows a slight upfield shift relative to free HBpin with resonances at 35.53 ppm and 34.21 ppm for free HBpin and 35.43 ppm and 34.00 ppm for the mixture. The upfield shift indicates that the boron is more shielded as the nitrogen contributes electrons to the boron center. Third, control reactions using only an aluminum center or the ligand result in low yields. The reaction between acteophenone and 1.2 equivalents HBpin catalyzed by 10 mol% $AlCl_3$ gives product in only 12% yield, whereas the hydroboration catalyzed by 10 mol% (TriNOx)H_3 results in a 9% yield. This suggests that both activation modes are necessary for productive catalysis. Overall, the experiments illustrated that the newly synthesized compound **7** can successfully catalyze the hydroboration of carbonyls through

cooperative catalysis, demonstrating new activation parameters that result in transition-metal-like catalysis.

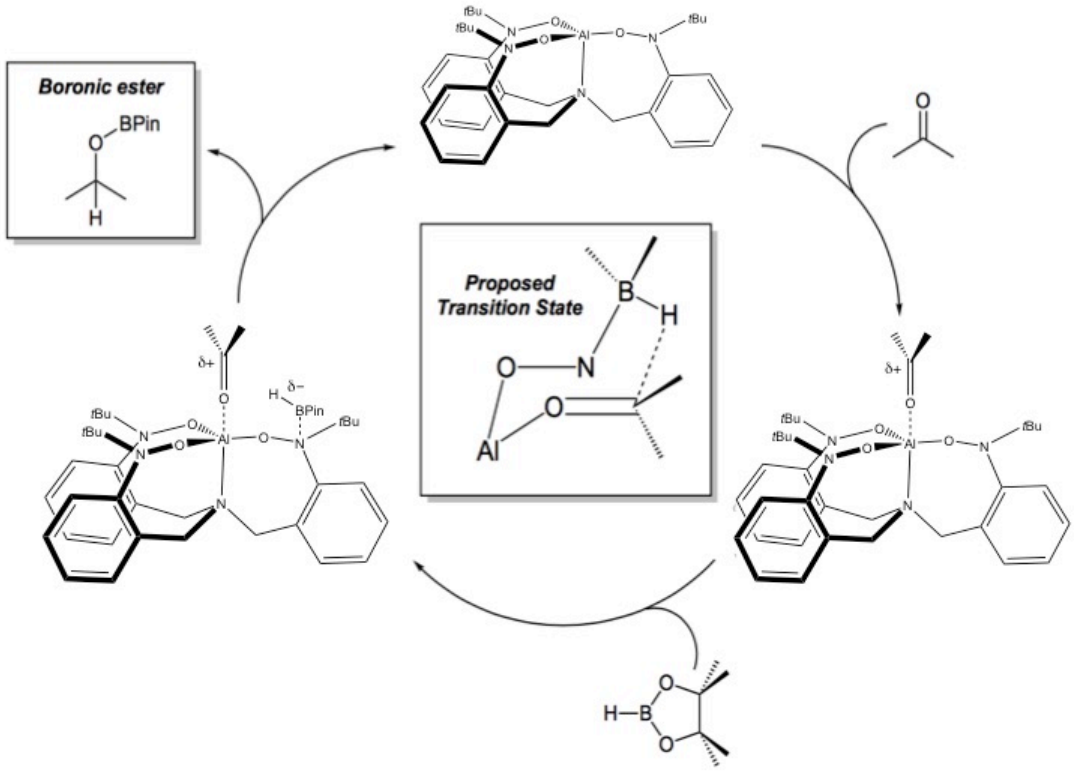

Scheme 11: Proposed catalytic cycle for the (TriNOx^{3-})Al-catalyzed carbonyl hydroboration.

3. Conclusion

Overall, aluminum, gallium, and indium complexes implementing a multidentate ligand incorporating multiple nitroxide functional groups have been synthesized. The cyclic voltammograms of both the aluminum and gallium complexes confirm the redox capabilities of both compounds. ($TriNOx^{3-}$)Al-py demonstrates two reversible redox events corresponding to sequential one-electron oxidations of the ligand, whereas ($TriNOx^{3-}$)Ga shows two non-reversible redox events. Further, the redox chemistry of the aluminum compound can be coupled with reaction chemistry as shown through successful one-electron oxidations, with oxidants such as XeF_2, CuCl, and [Fc][BPh_4]. Initial experiments have been performed using the same one-electron oxidants with ($TriNOx^{3-}$)Ga, which suggests that redox chemistry can be coupled to reaction chemistry. Future experiments will focus on continuing coupling redox chemistry and reaction chemistry in the gallium complex, as well as exploring two-electron oxidants for both aluminum and gallium compounds. The same concept should also be explored for ($TriNOx^{3-}$)In, as the solubility of the compound has prevented characterization through electrochemistry. The development of aluminum, gallium, and indium complexes using the same multidentate nitroxide-based ligand would provide a family of group 13 metals that vary in steric profiles, electronic parameters, and metal ionic radius, ultimately allowing the compound to be tuned for specific reactions.

Moreover, the dual nature of ($TriNOx^{3-}$)Al-py (**1**) opens the possibility of the compound to use metal-ligand cooperation for catalysis, which is enhanced by the removal of the pyridine to generate compound **7**. The Lewis basic sites on the nitrogen of the ligand arms in compound **7** in addition to the Lewis acidic metal center allow for

metal-ligand bifunctional catalysis that has been used toward the hydroboration of carbonyls. The catalyst can be used across a wide scope of substrates including both ketones and aldehydes and a mechanism has been proposed. The chemistry presented not only provides an example for the expansion of aluminum complexes, but how such complexes can be used as a viable catalyst in important organic reactions, enabling new activation parameters that result in transition-metal-like catalysis.

In the future, it would not only be beneficial to look at the kinetics of the hydroboration reactions catalyzed by compound **7**, but also to extend the use of the complex to other organic reactions. Extending research to investigate the catalytic ability of compound **7** in the hydroboration of imines, hydrosilylation of aldehydes and ketones, and its use in hydrogenations could be profitable, and again provide more environmentally and economically favorable options compared to the current systems.

4. Materials and Methods

4.1 Physical measurements

^{1}H and ^{13}C NMR spectra were recorded at ambient temperature using a Bruker 400 MHz spectrometer (399.78 MHz for ^{1}H, 100.52 MHz for ^{13}C, 376.17 MHz for ^{19}F, 128.38 MHz for ^{11}B). Chemical shifts were referenced to residual solvent. s = singlet, bs = broad singlet, d = doublet, q = quartet, td = triplet of doublets, m = multiplet, bm= broad multiplet, at = apparent triplet. Electrochemical measurements were done in a glovebox under a dinitrogen atmosphere using a CHI Potentiostat/Galvanostat. A glassy carbon working electrode, a platinum wire auxiliary electrode, and a silver wire plated with AgCl as a quasi-reference electrode were utilized. Potentials were reported versus ferrocene, which was added as an internal standard for calibration at the end of each run. Solutions employed during these studies were ~3 mM in analyte and 100 mM in [*n*-Pr_4N][BAr^F] (BAr_F^- = $B(3,5\text{-}CF_3)_2\text{-}C_6H_3)_4^-$) in ~5 mL of THF or MeCN. Data was collected in a positive-feedback IR compensation mode at 500 mV/s. Lewis acidity was calculated using the Gutmann-Beckett method. CHN analysis was performed at Midwestmicro Laboratory.

4.*2 Preparation of compounds*

All reactions and manipulations were performed under an inert atmosphere (N_2) using standard Schlenk techniques or in a Vacuum Atmospheres, Inc. NextGen drybox equipped with both oxygen and moisture purifier systems. Glassware was dried overnight at 150 °C before use. C_6D_6, $CDCl_3$, and C_5D_5N were degassed and stored over 4 Å molecular sieves prior to use. Tetrahydrofuran, toluene, dichloromethane, and pentane

were sparged for 20 min with dry argon and dried using a commercial two-column solvent purification system comprising two columns packed with neutral alumina (for tetrahydrofuran and dichloromethane) or Q5 reactant then neutral alumina (for hexanes, toluene, and pentane). Pyridine was purchased anhydrous and further dried over 4 Å molecular sieves prior to use. The $[\{(2\text{-}^{t}BuNO)C_6H_4CH_2\}_3N]H_3$ ligand precursor[26] and [*n*-Pr_4N][BAr^F] electrolyte[43] were prepared according to literature procedures. All other reagents were purchased from commercial sources and used as received.

*4.2.1 Synthesis of (TriNOx^{3-})Al-py (**1**)*

(TriNOx)H_3 (1.0 g, 1.8 mmol) was added to a flask equipped with a magnetic stir bar and dissolved in THF (~ 50 mL). $NaN(SiMe_3)_2$ (1.0 g, 5.5 mmol) was added to the stirring solution. The resulting reaction mixture was stirred at room temperature for 2 hours, after which aluminum chloride (0.24g, 1.8 mmol) was added. The solution was stirred for 12 hours after which the reaction products were filtered over a Celite-padded frit, which was subsequently washed with a liberal amount of THF. Volatiles were removed from the filtrate. Crude product was dissolved in pyridine and stirred for 40 minutes after which the solvents were removed from solution. The product was then dissolved in toluene and filtered over a Celite-padded frit. Solvents were removed from the filtrate to give (TriNOx^{3-})Al-py as a tan solid. Yield: 0.91 g, 1.4 mmol (77%). Crystals suitable for X-ray diffraction were obtained from cooling a saturated pyridine solution at –25°C. ^{1}H NMR (C_6D_6): δ 8.57 (bs, 2H), 7.57 (d, J = 8.0 Hz, 3H), 7.02 (td, J = 8.0 Hz, J = 1.6 Hz, 3H), 6.96 (m, 4H), 6.86 (td, J = 6.8 Hz, J = 0.4 Hz, 3H), 6.66 (m, 2H), 4.71 (d, J = 11.2 Hz, 3H, NCH_2), 2.83 (d, J = 11.2 Hz, 3H, NCH_2), 1.44 (s, 27 H,

$C(CH_3)_3$). ^{13}C NMR (C_6D_6):δ 152.9, 150.3, 135.2, 133.4, 132.3, 129.5, 124.7, 124.4, 123.5, 61.8, 58.7, 28.1 (C(CH 3) 3). Anal. Calcd. for $C_{38}H_{50}AlN_5O_3$: C, 70.02; H, 7.73; N, 10.74 Found: C, 69.51; H, 7.70; N, 9.91.

*4.2.2 Synthesis of (TriNOx^{3-})Ga (**2**)*

(TriNOx)H_3 (0.20 g, 0.36 mmol) was added to a flask equipped with a magnetic stir bar and dissolved in THF (~ 25 mL). $NaN(SiMe_3)_2$ (0.23 g, 1.2 mmol) was added to the stirring solution. The resulting reaction mixture was stirred at room temperature for 2 hours, after which gallium chloride (0.064 g, 0.36 mmol) was added. The solution was stirred for 12 hours after which the reaction products were filtered over a Celite-padded frit and volatiles were removed from the filtrate. Crude product was dissolved in pyridine and stirred for 40 minutes after which the solvents were removed from solution. The product was then dissolved in dichloromethane and filtered over a Celite-padded frit. Solvents were removed from the filtrate to give (TriNOx^{3-})Ga as a tan solid. Yield: 0.18 g, 0.29 mmol (79%). ^1H NMR (C_6D_6): δ 7.63 (d, J= 7.6 Hz, 3H), 7.07 (m, 3H), 7.02 (m, 3H), 6.92 (m, 3H), 4.87 (d, 3H, J=11.4 Hz), 2.85 (d, 3H, J=11.4 Hz), 1.41 (s, 27H). ^{13}C NMR (C_6D_6): δ 152.96, 133.52, 132.53, 129.80, 125.22, 124.80, 62.48, 58.55, 28.06.

*4.2.3 Synthesis of (TriNOx^{3-})In (**3**)*

$[In(NEt_2)_3]_2$ (0.21 g, 0.32 mmol) was added to a flask equipped with a magnetic stir bar and dissolved in toluene (~ 30 mL). (TriNOx)H_3 (0.35 g, 0.64 mmol) was added to the stirring solution. The resulting reaction mixture was stirred at room temperature for 12 hours. Pyridine (~15 mL) was added and the solution was stirred for 1 hour, after

which the solvents were removed. The crude product was then heated in pyridine until the solution was homogeneous, cooled to room temperature and placed in the freezer at –25°C for 24 hours. ($TriNOx^{3-}$)In crashed out of solution as a white powder. Yield: 0.12 g, 0.29 mmol (57%). ^{1}H NMR (C_5D_5N): 7.84 (d, 3H, J= 8.0 Hz), 7.42 (m, 6H), 7.25 (m, 3H), 5.14 (d, 3H, J=10.7), 2.58 (d, 3H, J=10.8), 0.99 (s, 27H). ^{13}C NMR (C_5D_5N): 152.83, 134.57, 132.85, 128.82, 127.94, 124.90, 60.39, 59.71, 26.19. Anal. Calcd. for $C_{33}H_{45}InN_4O_3$: C, 60.00; H, 6.87; N, 8.48 . Found: C, 59.67 ; H, 6.70 ; N, 8.27 .

*4.2.4 Synthesis (TriNOx)Al-F (**4**)*

($TriNOx^{3-}$)Al-py (0.10 g, 0.15 mmol) was added to a vial equipped with a magnetic stir bar and dissolved in THF (~15 mL). XeF_2 (0.026 g, 0.15 mmol) was added to the stirring solution. The resulting mixture was stirred at room temperature for 12 hours after which the reaction was filtered over a Celite-padded frit and solvents removed. The crude product was dissolved in dichloromethane (~10 mL) and filtered over a Celite-padded frit. Solvents were removed from the filtrate to give ($TriNOx^{2-}$)Al-F as a tan solid. Yield: 0.07 g, 0.12 mmol (77%). Compound is NMR silent. Anal. Calc. for $C_{33}H_{45}AlFN_4O_3$: C, 66.98; H, 7.67; N, 9.47. Found: C, 66.57; H, 7.73; N, 9.00.

*4.2.5 Synthesis of [(TriNOx)Al][BPh_4] (**5**)*

($TriNOx^{3-}$)Al-py (0.10 g, 0.15 mmol) was added to a vial equipped with a magnetic stir bar and dissolved in THF (~15 mL). [Fc][BPh_4] (0.077 g, 0.15 mmol) was added to the stirring solution. The resulting mixture was stirred at room temperature for 12 hours after which the reaction was filtered over a Celite-padded frit and solvents

removed. The crude product was stirred in hexane (~ 5 min) after which the solution was filtered over a medium frit to give [(TriNOx^{2-})Al][BPh_4] as a tan solid. Yield: 0.09 g, 0.093 mmol (58%). Compound is NMR silent. Anal. Calc. for $C_{57}H_{65}AlBN_4O_3$: C, 76.76; H, 7.35; N, 6.28. Found: C, 74.13; H, 7.35; N, 6.02.

*4.2.6 Synthesis of (TriNOx)Al-Cl (**6**)*

(TriNOx^{3-})Al-py (0.15 g, 0.23 mmol) was added to a vial equipped with a magnetic stir bar and dissolved in toluene (~15 mL). CuCl (0.039 g, 0.39 mmol) was added to the stirring solution. The resulting mixture was stirred at room temperature for 12 hours after which the reaction was filtered over a Celite-padded frit and solvents removed. The crude product dissolved in dichloromethane (~ 20 mL) and filtered over a Celite-padded frit. Solvents were removed from the filtrate. (TriNOx^{2-})Al-Cl crashed out as a tan solid from a slow evaporation of THF and hexane. Yield: 0.072 g, 0.12 mmol (51%.) Compound is NMR silent.

*4.2.7 Synthesis of (TriNOx^{3-})Al (**7**)*

(TriNOx)H_3 (1.0 g, 1.8 mmol) was added to a flask equipped with a magnetic stir bar and dissolved in THF (~ 50 mL). NaN($SiMe_3$)$_2$ (1.0 g, 5.5 mmol) was added to the stirring solution. The resulting reaction mixture was stirred at room temperature for 2 hours, after which aluminum chloride (0.24g, 1.8 mmol) was added. The solution was stirred for 12 hours after which the reaction products were filtered over a Celite-padded frit, which was subsequently washed with a liberal amount of THF. Volatiles were removed from the filtrate. The product was then dissolved in toluene and filtered over a

Celite-padded frit. Solvents were removed from the filtrate to give ($TriNOx^{3-}$)Al as a tan solid. Yield: 0.76 g, 1.3 mmol (74%).

4.3 General Hydroboration Protocol

($TriNOx^{3-}$)Al (28.6 mg, 0.05 mmol for ketones; 14.3 mg, 0.025 mmol for aldehydes) and hexamethylcyclotrisiloxane (18.5, 0.083 mmol) were weighed into a vial equipped with a magnetic stir bar and were dissolved in $CDCl_3$ (1.0 mL). Carbonyl substrate (0.5 mmol) was added to the stirring mixture followed by pinacolborane (87 μL, 0.6 mmol). The reaction was stirred at room temperature until being analyzed by ^1H NMR spectroscopy at the indicated time.

Supplementary Information

X-Ray Structure determination and refinement parameters for (TriNOX^{3-})Al-py (compound 1).

X-ray diffraction data were collected on a Bruker APEXII[44] CCD area detector employing graphite-monochromated Mo-Kα radiation (λ=0.71073Å) at 100 K. Rotation frames were integrated using SAINT,[45] producing a listing of unaveraged F^2 and $\sigma(F^2)$ values which were then passed to the SHELXTL[46] program package for further processing and structure solution. The intensity data were corrected for Lorentz and polarization effects and for absorption using SADABS[47] and the structures were solved by direct methods (SHELXT[48]) and refined by full-matrix least squares based on F^2 using SHELXL-97.[49] All non-hydrogen atoms were refined anisotropically and hydrogen atoms were refined using a riding model.

Further details for the refinement of (TriNOx^{3-})Al-py (1) (CCDC 1862706): The TriNOx ligand is disordered; the two contributing disorder structures are mirror images of each other as shown in the graphic below:

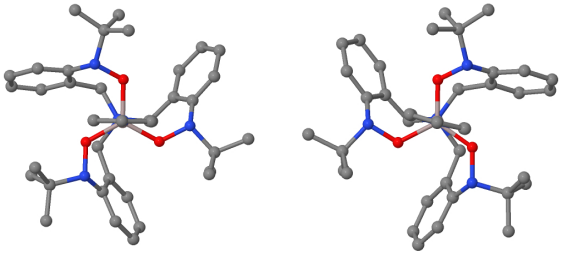

The occupancies of the two TriNOx disorder models refined to 0.838(1)/0.162(1). The coordinated pyridine was also disordered by a small rotation about the Al-py axis with occupancies of 0.61(4)/0.39(4). Refinement converged to R1=0.0454 and wR2=0.1106 for 6378 observed reflections for which F > 4σ(F) and R1=0.0638 and wR2=0.1216 and GOF =1.149 for all 8149 unique, non-zero reflections and 837 variables.

Table S1. Summary of Structure Determination of (TriNOx^{3-})Al-py (**1**)

Empirical formula	$C_{38}H_{50}N_5O_3Al$
Formula weight	651.81
Temperature	100(1) K
Wavelength	0.71073 Å
Crystal system	monoclinic
Space group	C2/c
Cell constants:	
a	29.6452(16) Å
b	12.8416(7) Å
c	19.2768(10) Å
β	104.904(3)°
Volume	7091.6(7) Å^3
Z	8
Density (calculated)	1.221 Mg/m^3
Absorption coefficient	0.101 mm^{-1}
F(000)	2800
Crystal size	0.23 x 0.15 x 0.15 mm^3
Theta range for data collection	1.42 to 27.53°
Index ranges	$-38 \le h \le 38$, $-16 \le k \le 16$, $-25 \le l \le 24$
Reflections collected	115031
Independent reflections	8149 [R(int) = 0.0482]
Max. and min. transmission	0.7456 and 0.6891
Data / restraints / parameters	8149 / 1446 / 837
Goodness-of-fit on F^2	1.149
Final R indices [I>2sigma(I)]	R1 = 0.0454, wR2 = 0.1106
R indices (all data)	R1 = 0.0638, wR2 = 0.1216
Largest diff. peak and hole	0.290 and -0.250 e.Å^{-3}

Table S2. Selected solid-state and calculated bond distances (Å) and angles (°) for the ($TriNOx^{3-}$)Al-py (**1**) complex.

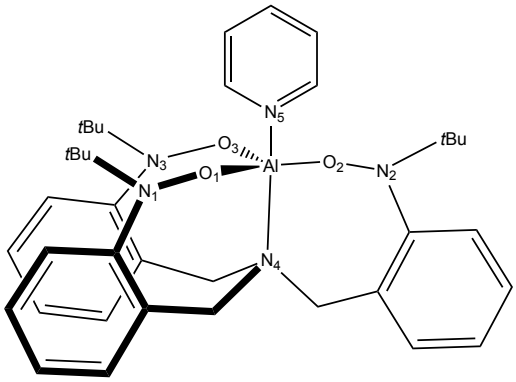

	Solid-State	DFT
Al(1)-O(1)	1.755(3)	1.811
Al(1)-O(2)	1.758(4)	1.815
Al(1)-O(3)	1.770(3)	1.814
Al(1)-N(4)	2.1655(13)	2.161
Al(1)-N(5)	2.046(10)	2.088
N(1)-O(1)	1.448(3)	1.462
N(2)-O(2)	1.438(5)	1.457
N(3)-O(3)	1.435(3)	1.465
O(1)-Al-O(3)	119.69(11)	119.44
O(1)-Al(1)-O(2)	121.95(16)	121.99
O(2)-Al(1)-O(3)	116.89(17)	118.00
O(1)-Al(1)-N(4)	86.65(14)	86.21
O(2)-Al(1)-N(4)	86.28(19)	87.97
O(3)-Al(1)-N(4)	84.93(12)	88.28
O(1)-Al(1)-N(5)	91.7(4)	93.20
O(2)-Al(1)-N(5)	98.9(5)	90.50
O(3)-Al(1)-N(5)	91.4(5)	93.74
N(4)-Al(1)-N(5)	174.6(4)	176.66

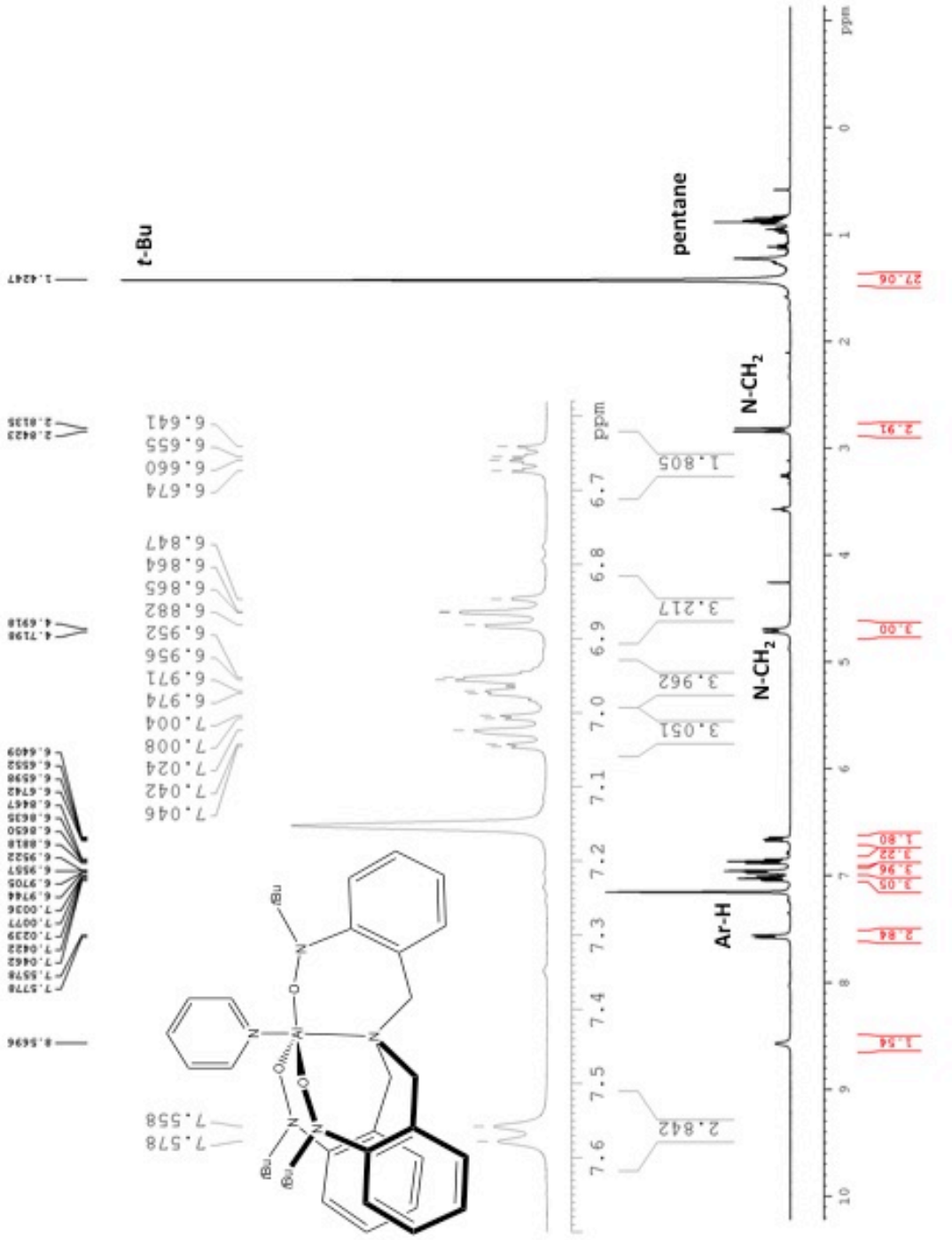

Figure S1. ^{1}H NMR spectrum of (TriNOx^{3-})Al-py (**1**) in C_6D_6 at 25 ºC.

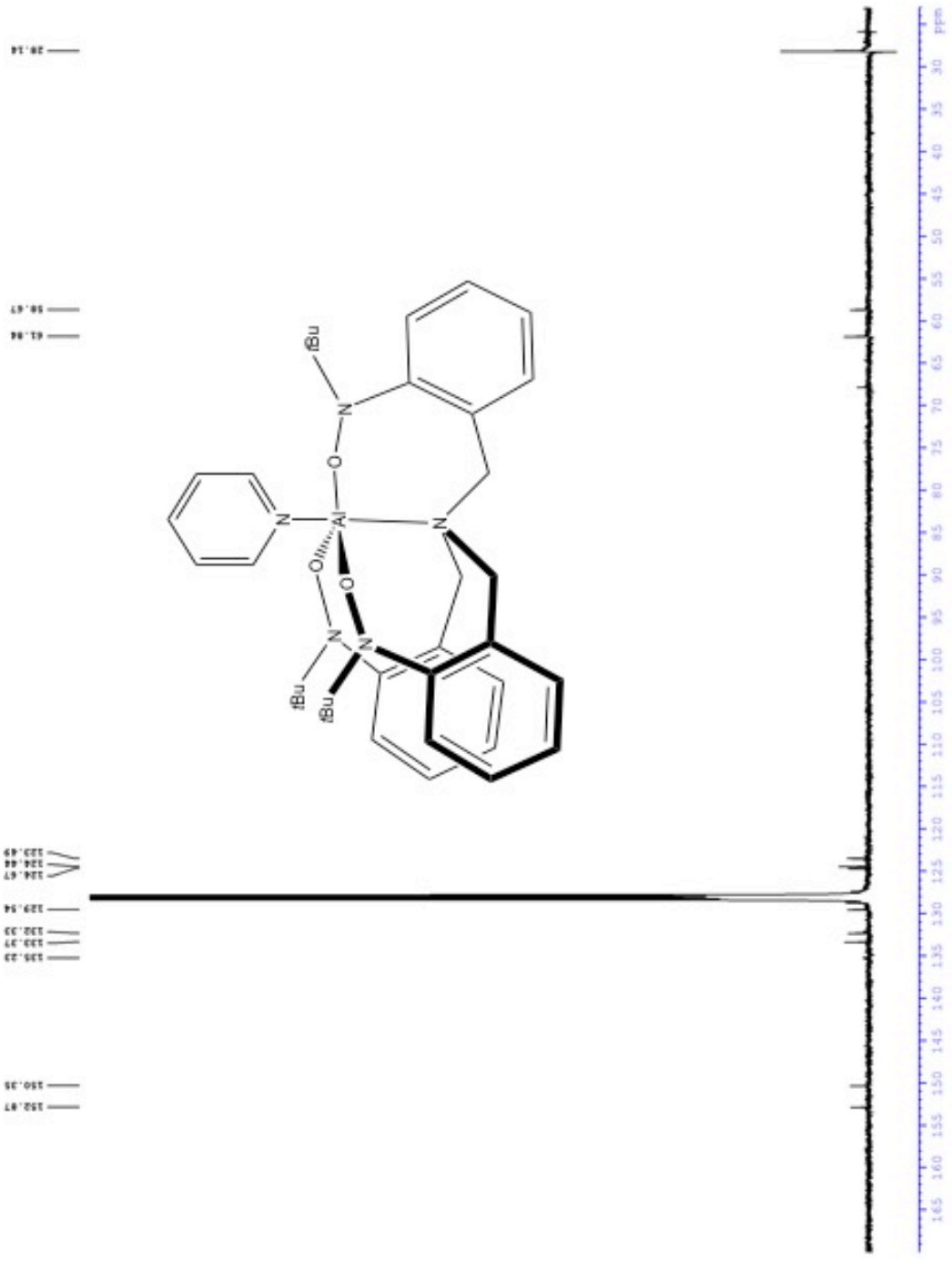

Figure S2. $^{13}C\{^{1}H\}$ NMR spectrum of ($TriNOx^{3-}$)Al-py (**1**) in C_6D_6 at 25 ºC.

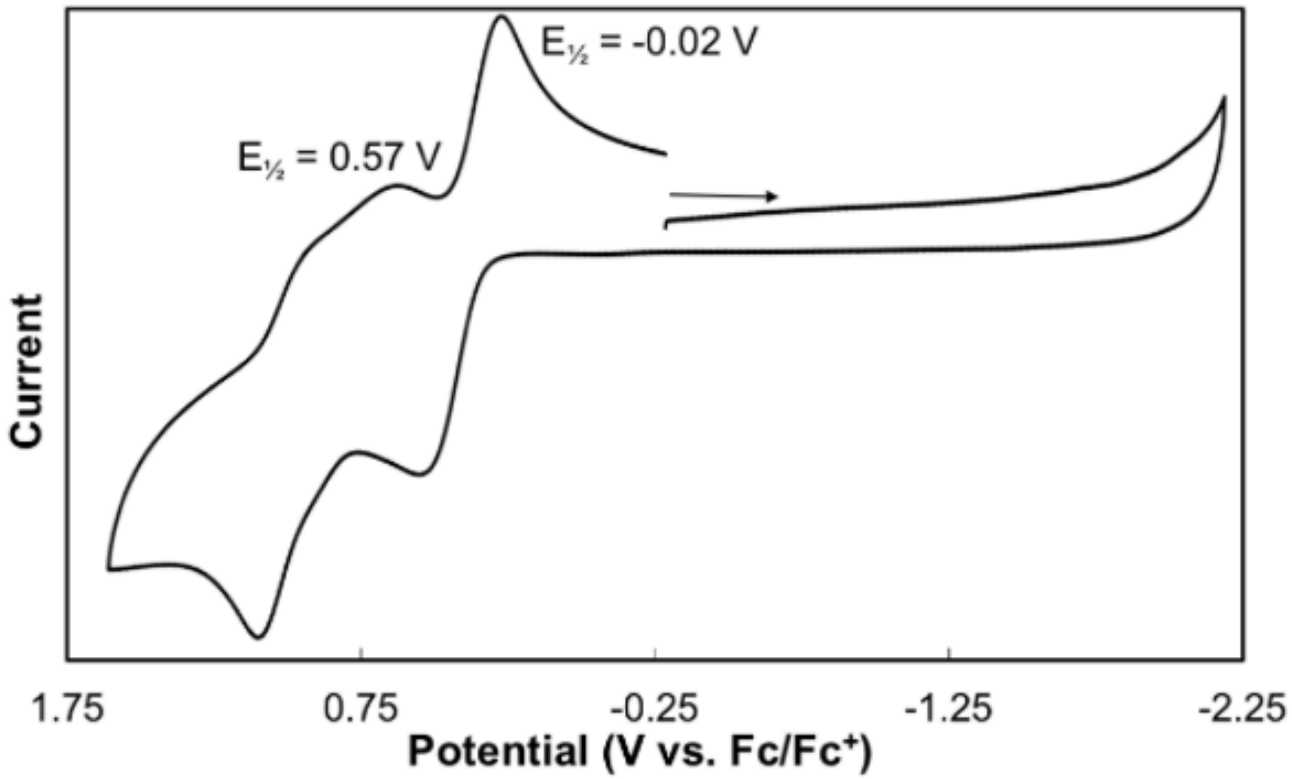

Figure S3: Cyclic voltammogram of (TriNOx^{3-})Al-py (**1**) recorded in 0.1 M [*n*-Pr$_4$N][BAr$_F$] THF solution recorded at 500 mV/s.

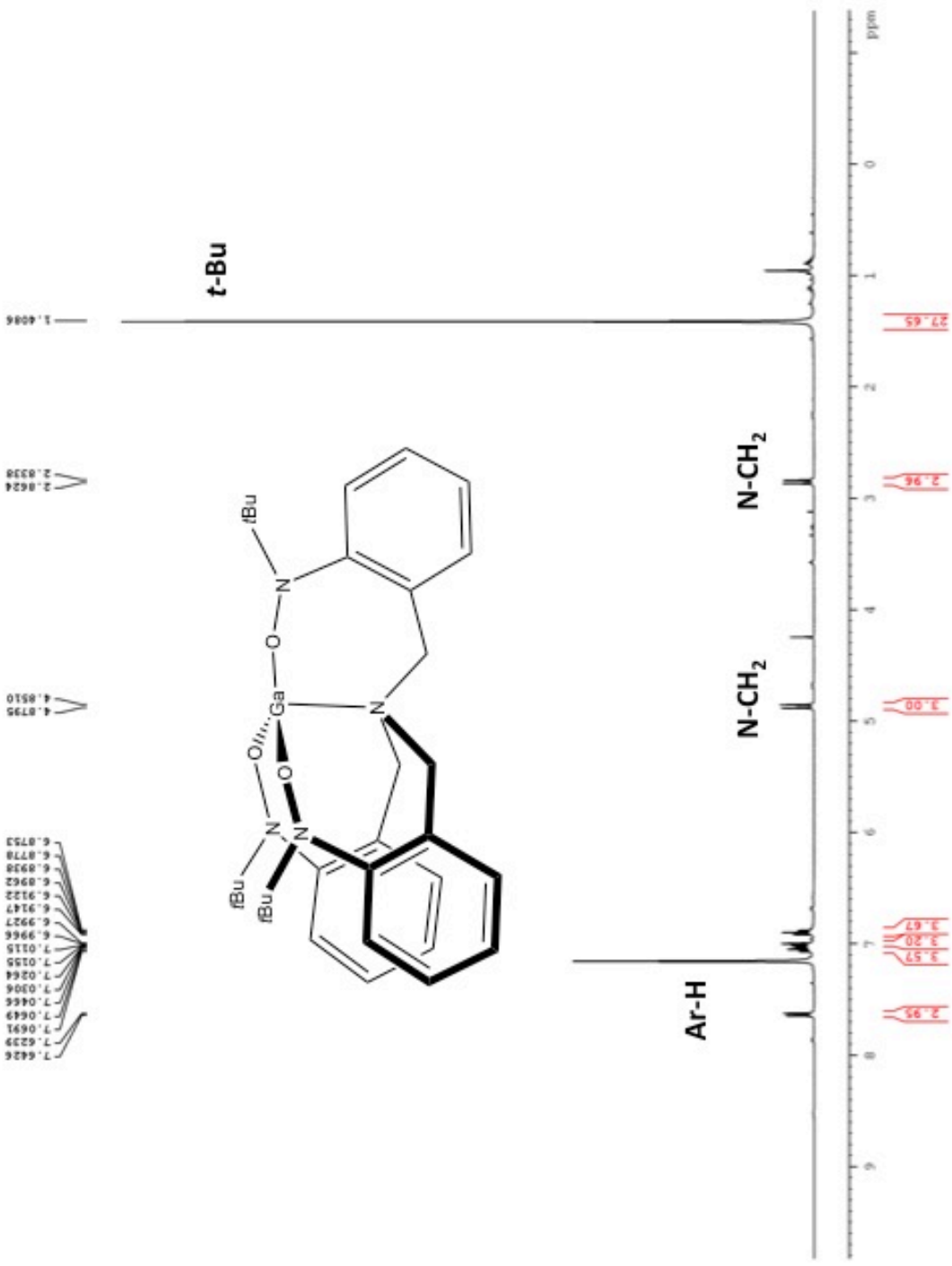

Figure S4. ^{1}H NMR spectrum of (TriNOx^{3-})Ga-py (**2**) in C_6D_6 at 25 ºC.

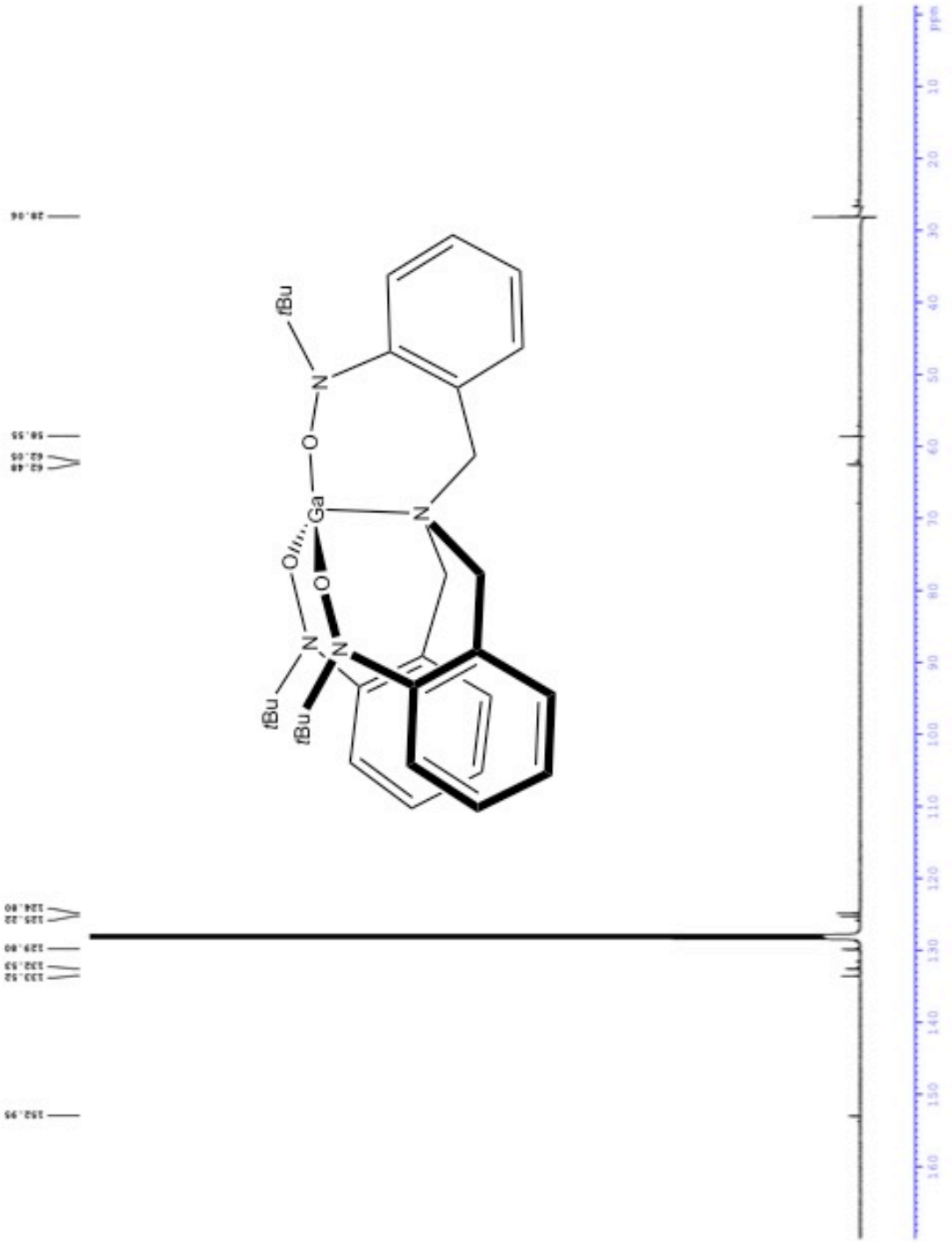

Figure S5. $^{13}C\{^{1}H\}$ NMR spectrum of (TriNOx^{3-})Ga-py (**2**) in C_6D_6 at 25 ºC.

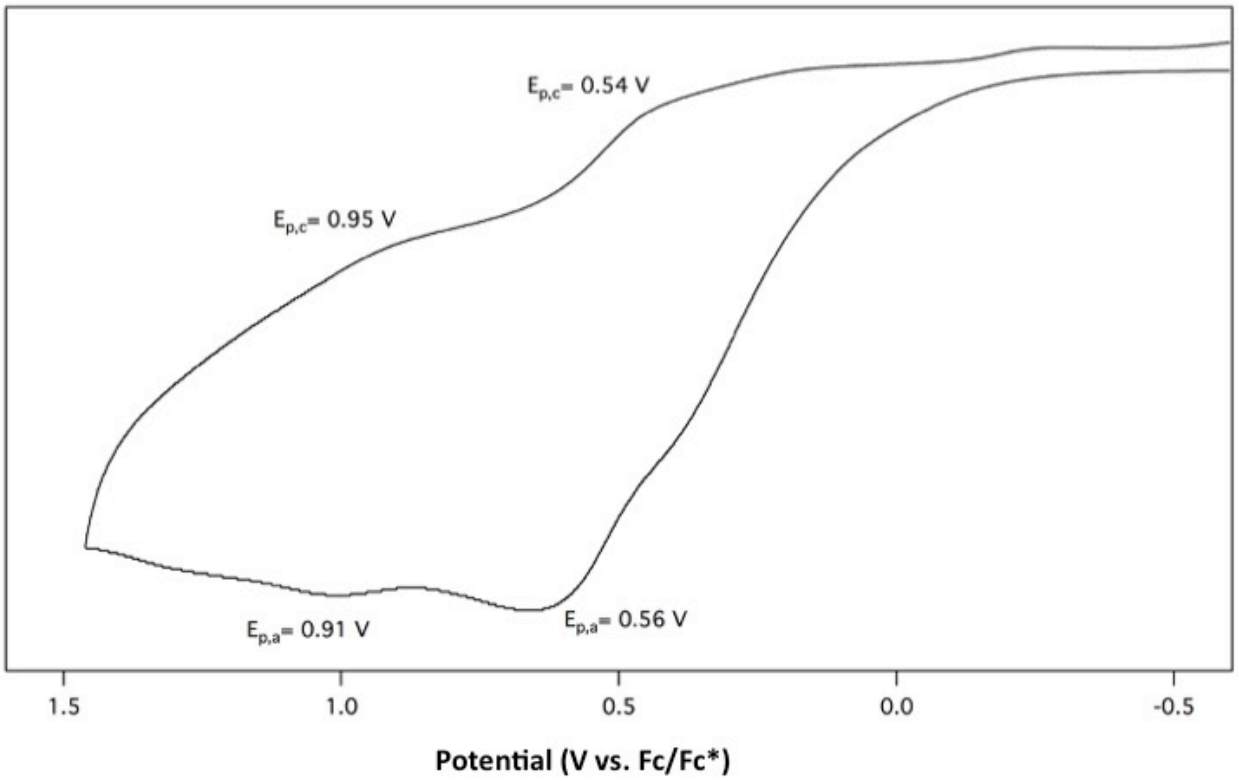

Figure S6: Cyclic voltammogram of (TriNOx^{3-})Ga (**2**) recorded in 0.1 M [*n*-Pr_4N][BAr_F] MeCN solution recorded at 500 mV/s.

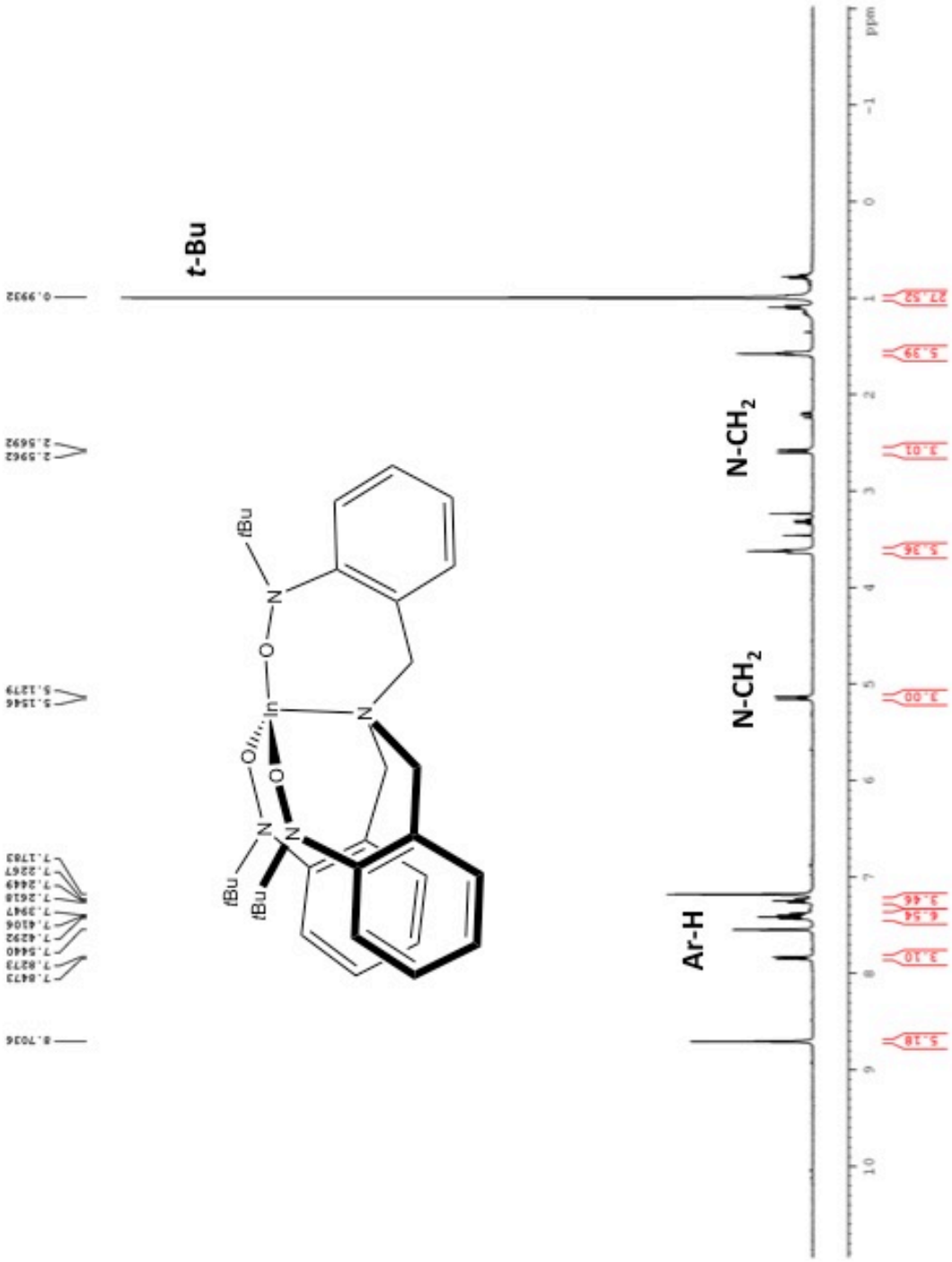

Figure S7. ^{1}H NMR spectrum of (TriNOx^{3-})In-py (**3**) in C_5D_5N at 25 ºC.

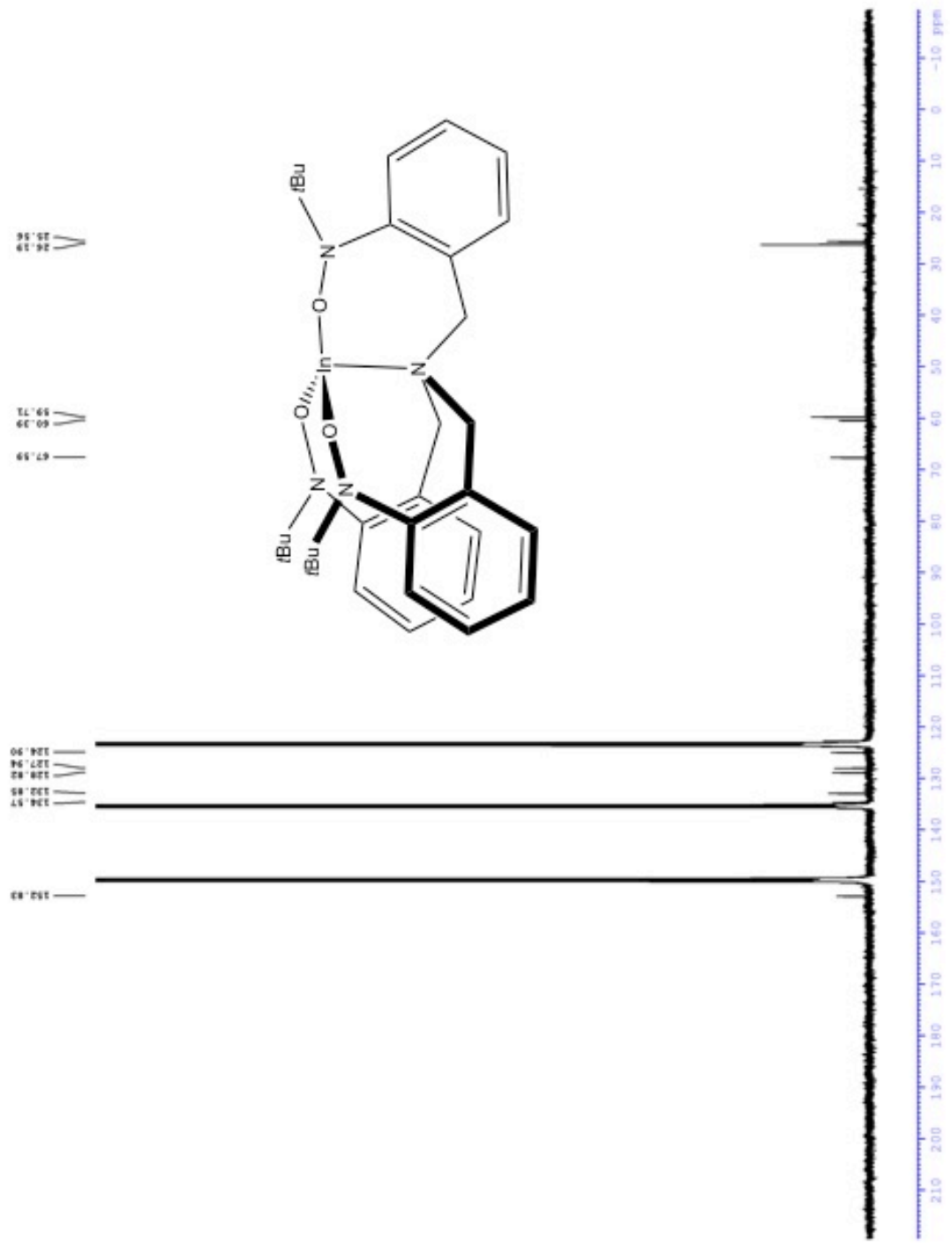

Figure S8. $^{13}C\{^{1}H\}$ NMR spectrum of ($TriNOx^{3-}$)In-py (**3**) in C_5D_5N at 25 ºC

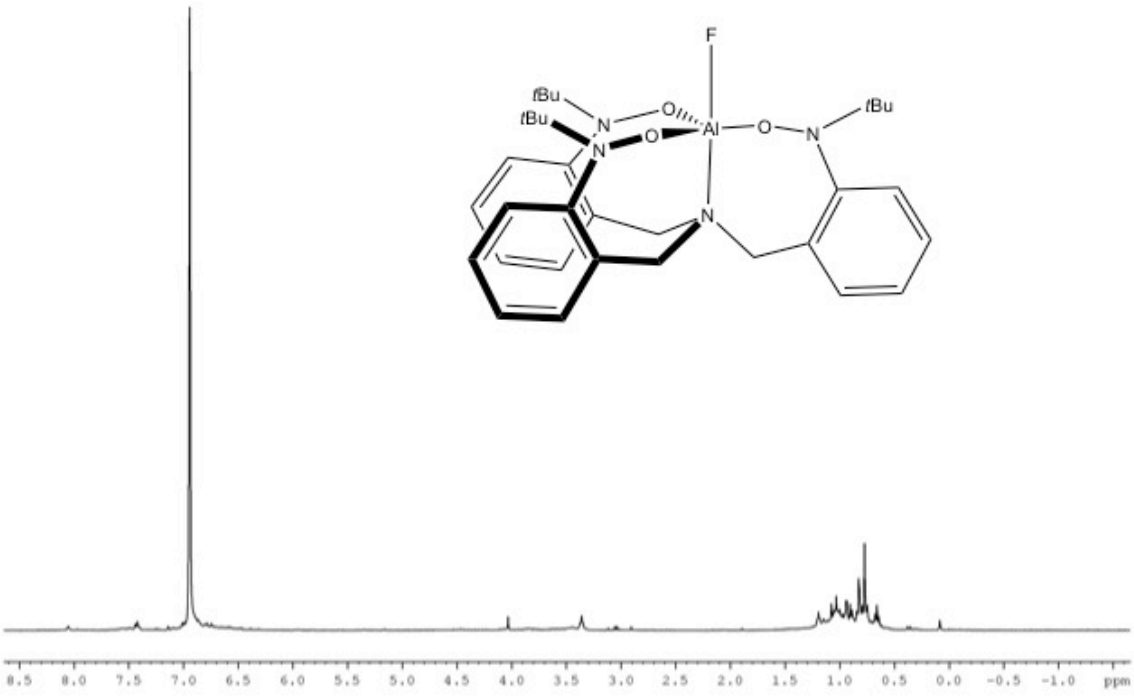

Figure S9. ^{1}H NMR spectrum of (TriNOx^{2-})Al-F (**4**) in C_6D_6 at 25 ºC.

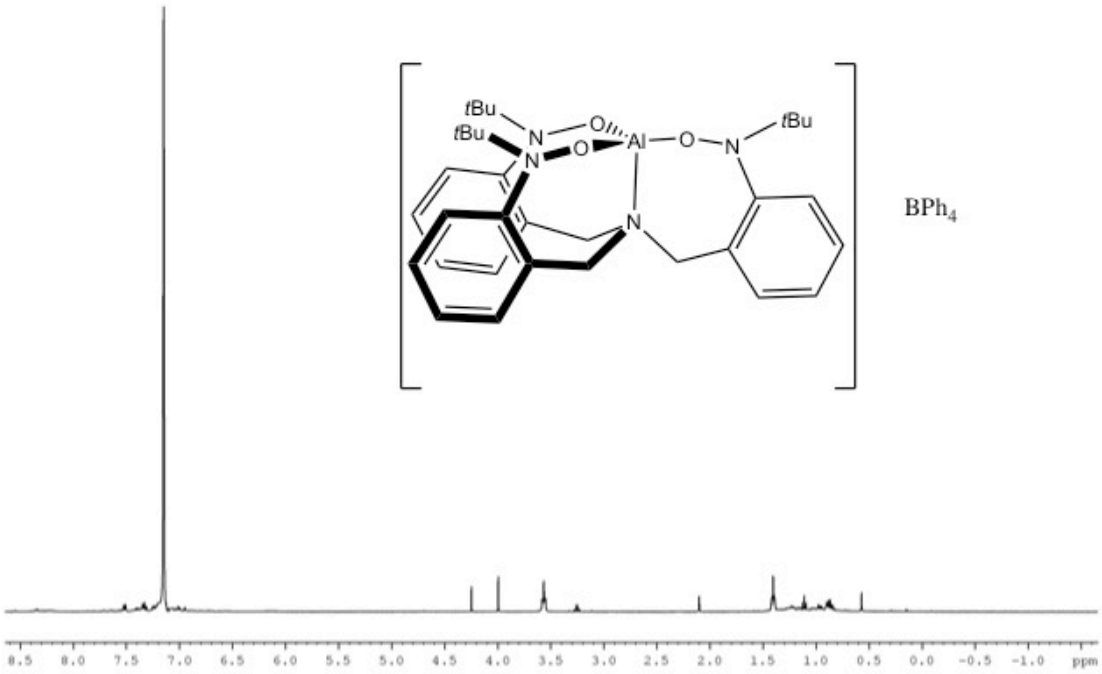

Figure S10. ^{1}H NMR spectrum of [(TriNOx^{2-})Al][BPh_4] (**5**) in C_6D_6 at 25 ºC.

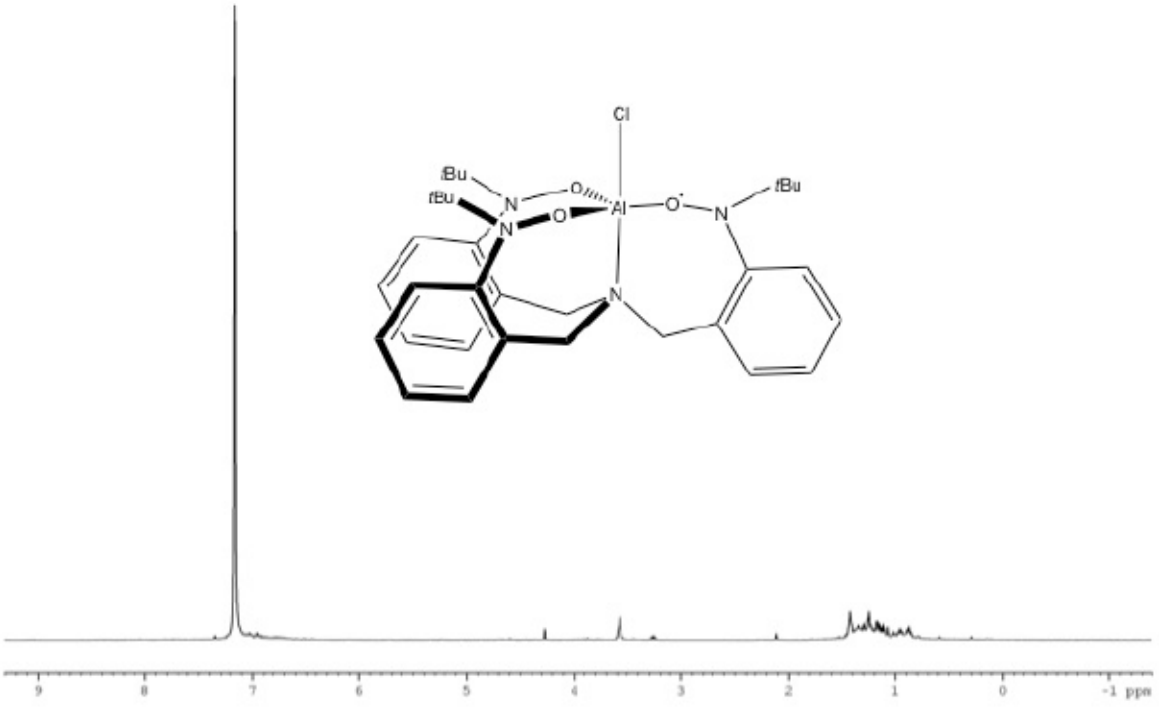

Figure S11. ^{1}H NMR spectrum of (TriNOx^{2-})Al-Cl (**6**) in C_6D_6 at 25 °C.

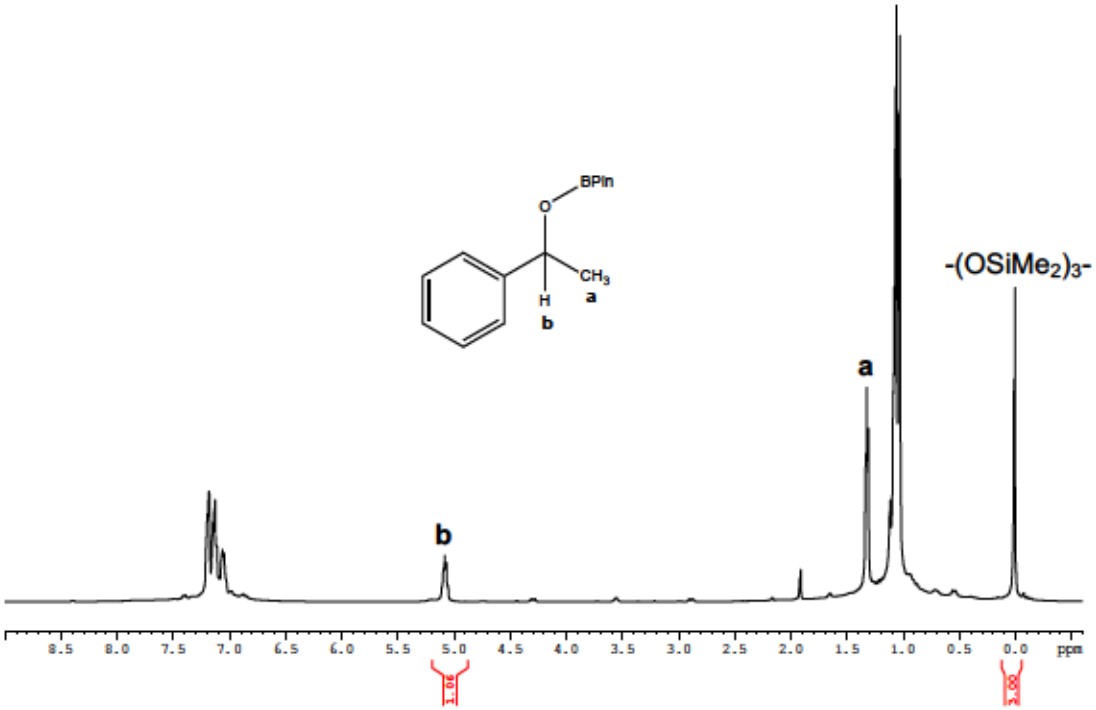

Figure S12. ^{1}H NMR spectra of the reaction products of the hydroboration of acetophenone with HBPin to give boronate ester **i** under optimized conditions.

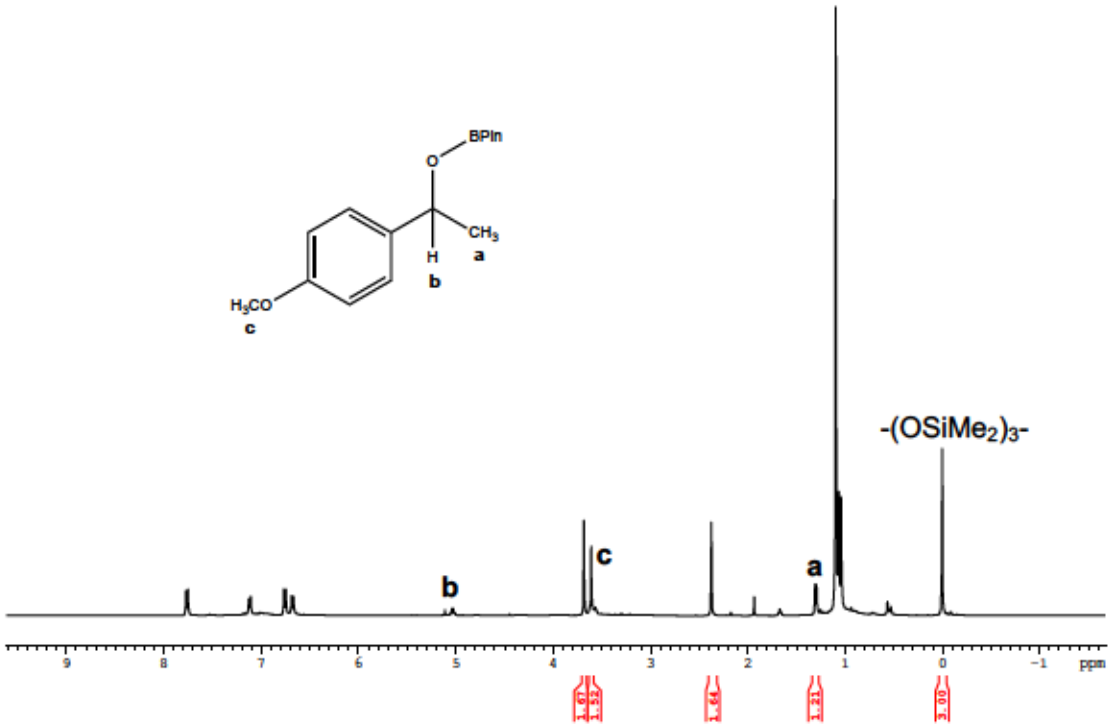

Figure S13. ^{1}H NMR spectra of the reaction products of the hydroboration of 4-methoxyacetophenone with HBPin to give boronate ester **ii** under optimized conditions.

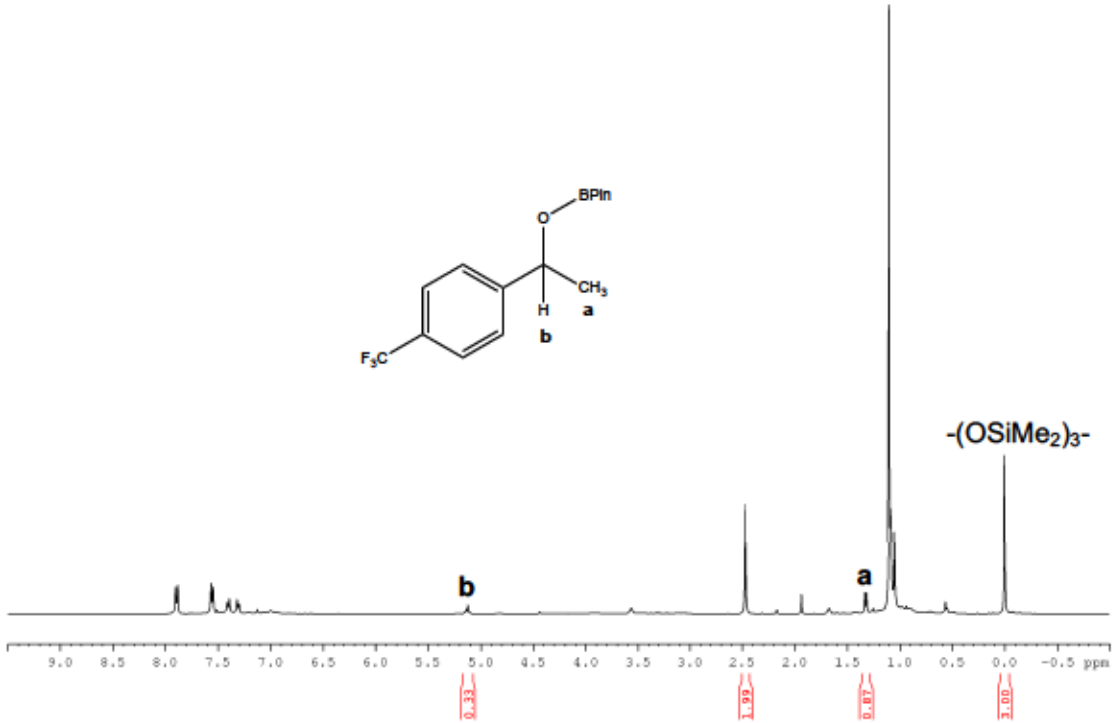

Figure S14. ^{1}H NMR spectra of the reaction products of the hydroboration of 4-trifluoromethylacetophenone with HBPin to give boronate ester **iii** under optimized conditions.

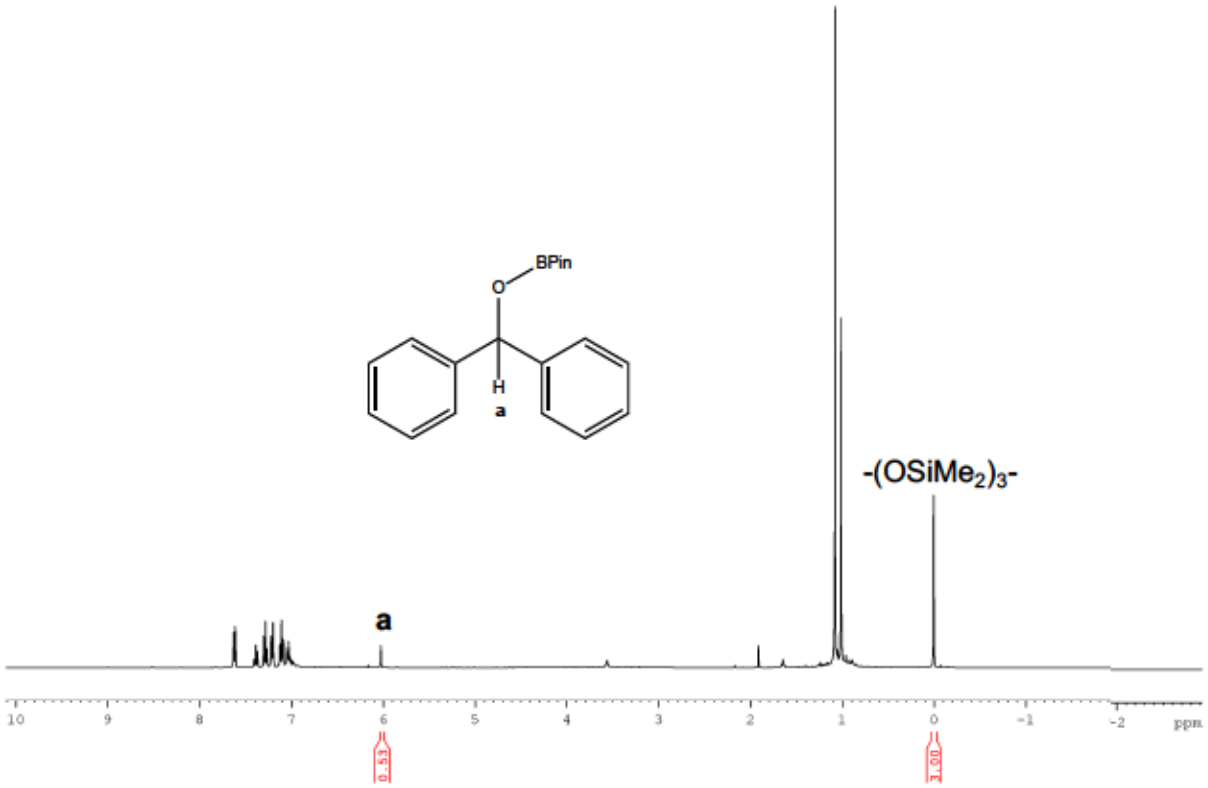

Figure S15. ^{1}H NMR spectra of the reaction products of the hydroboration of benzophenone with HBPin to give boronate ester **iv** at 75 °C under optimized conditions.

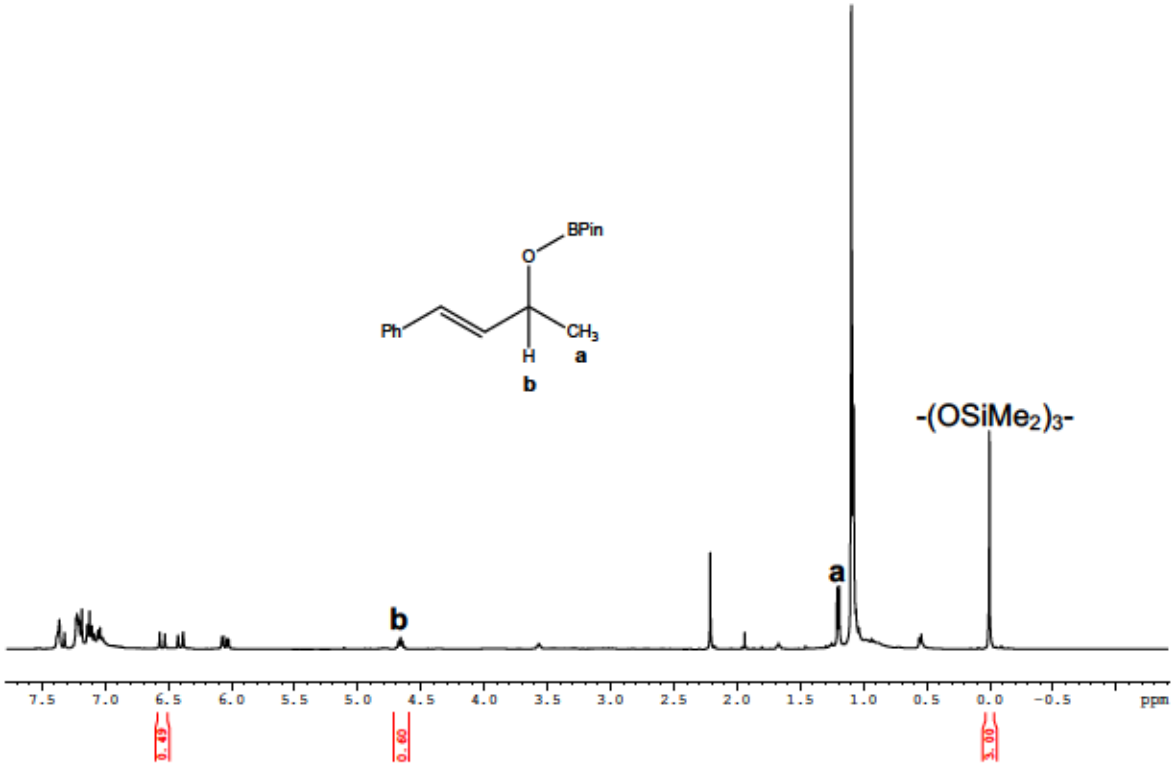

Figure S16. ^{1}H NMR spectra of the reaction products of the hydroboration of benzylideneacetone with HBPin to give boronate ester **v** under optimized conditions.

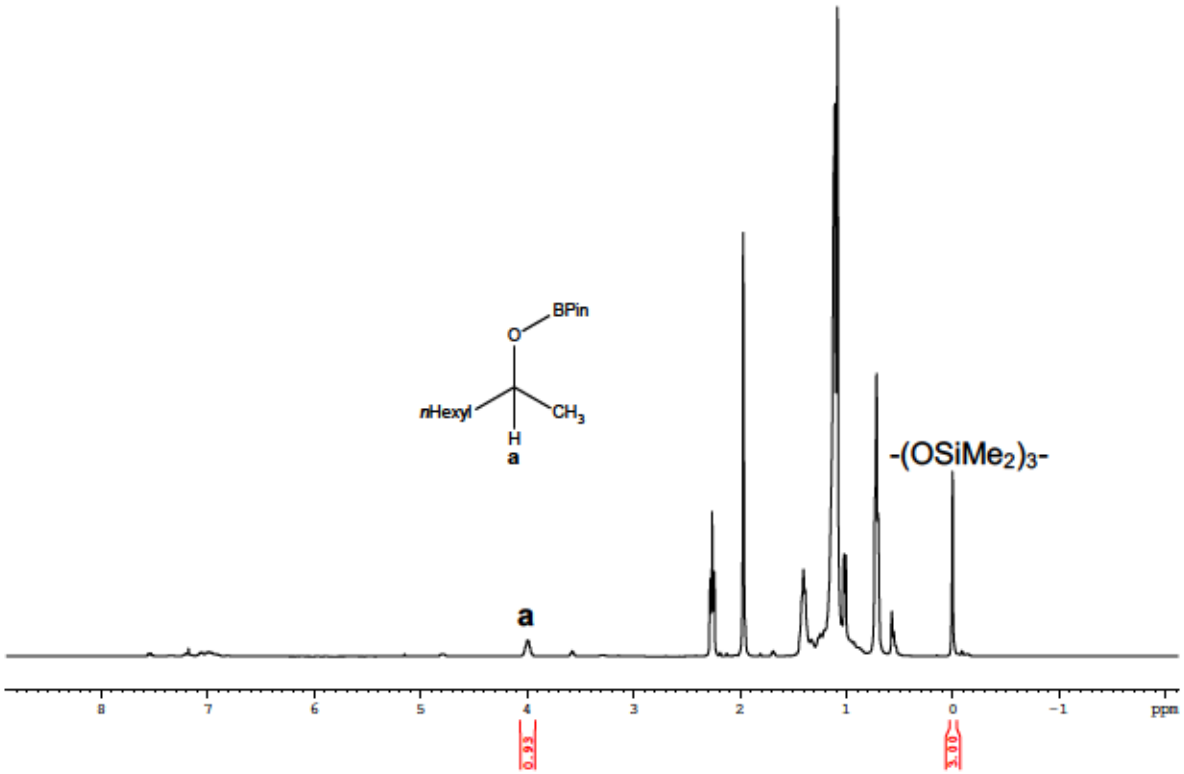

Figure S17. ^{1}H NMR spectra of the reaction products of the hydroboration of 2-octanone with HBPin to give boronate ester **vi** under optimized conditions.

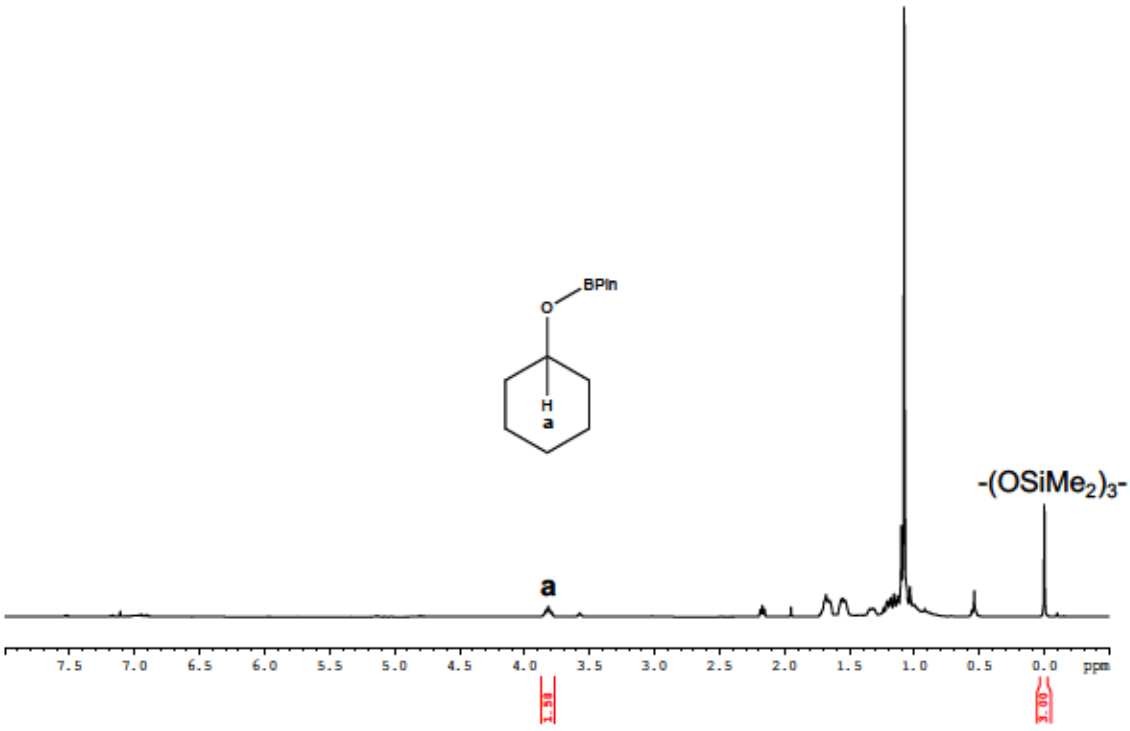

Figure S18. ^{1}H NMR spectra of the reaction products of the hydroboration of cyclohexanone with HBPin to give boronate ester **vii** under optimized conditions.

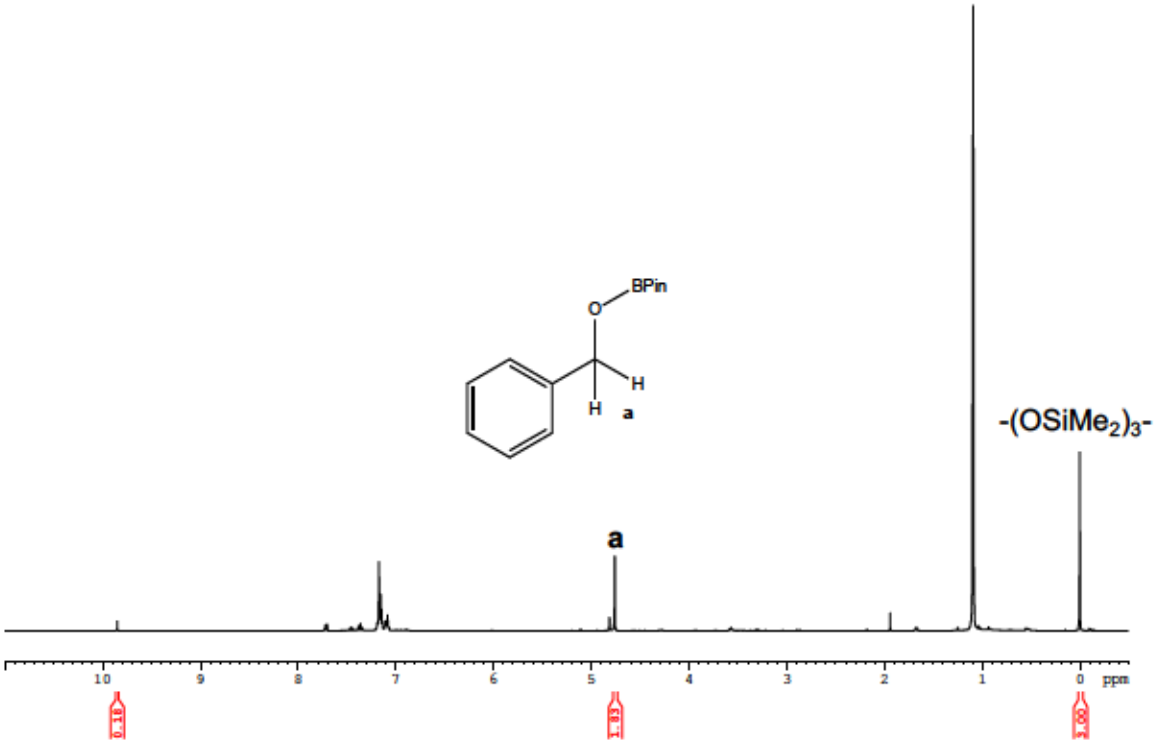

Figure S19. ^{1}H NMR spectra of the reaction products of the hydroboration of benzaldehyde with HBPin to give boronate ester **viii** under optimized conditions.

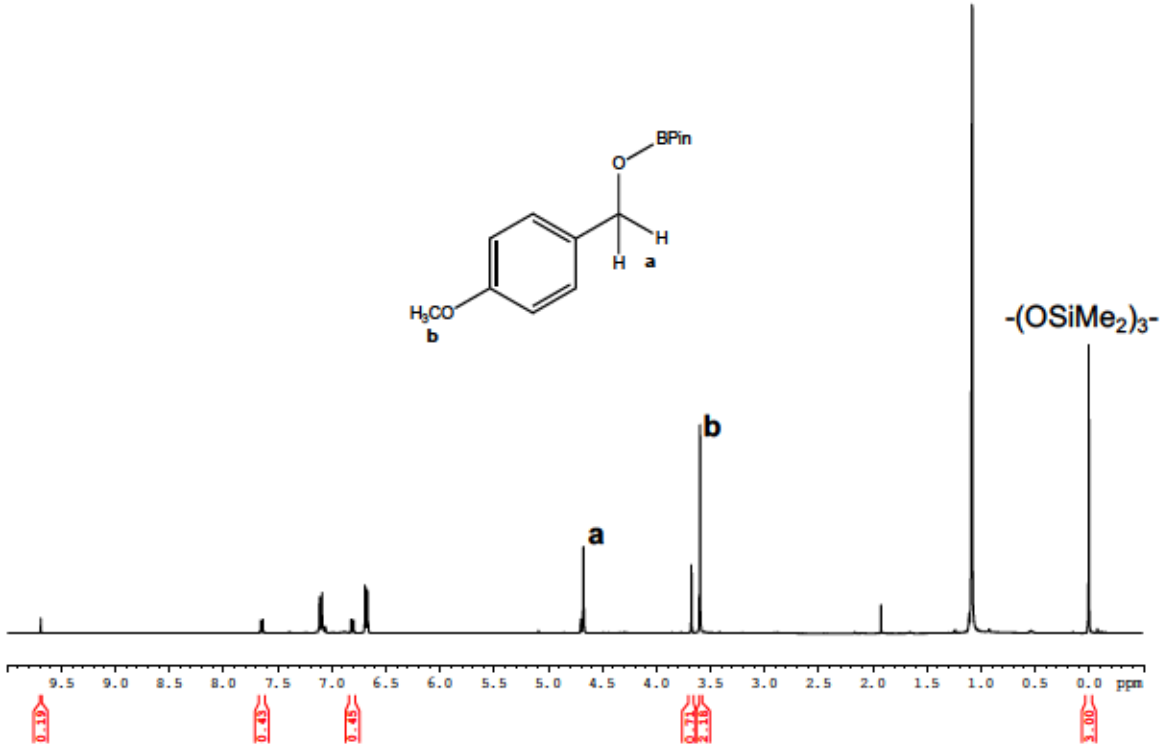

Figure S20. ^{1}H NMR spectra of the reaction products of the hydroboration of p-anisaldehyde with HBPin to give boronate ester **ix** under optimized conditions.

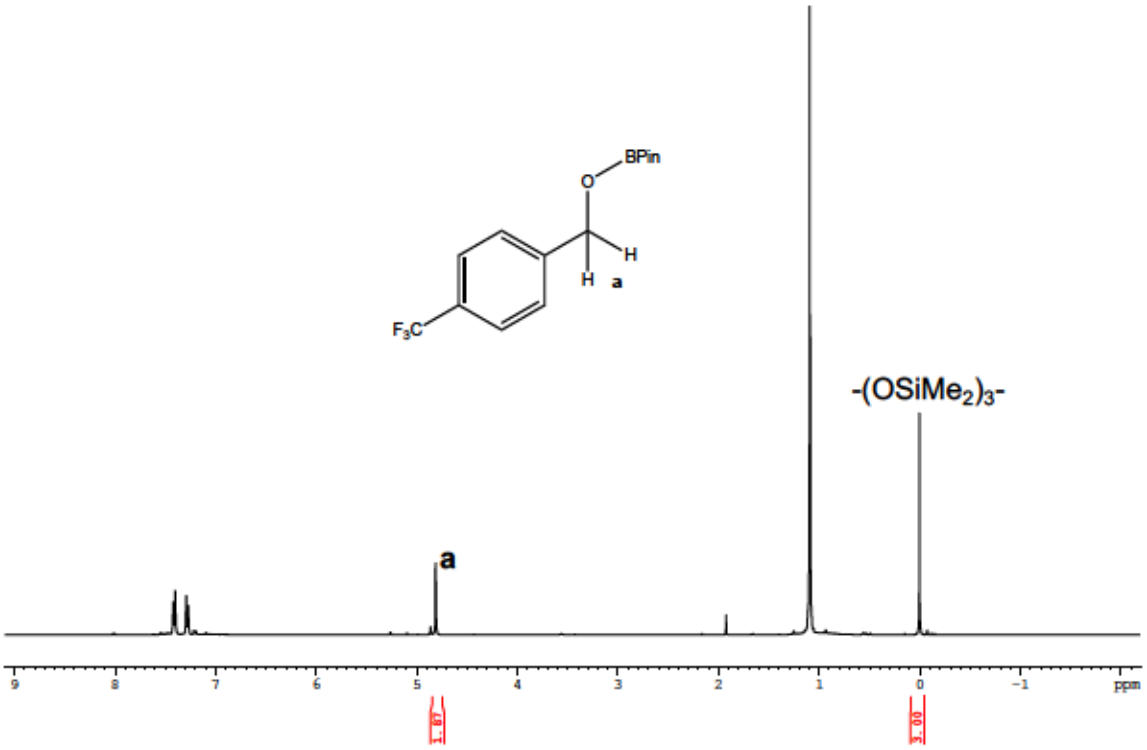

Figure S21. ^{1}H NMR spectra of the reaction products of the hydroboration of 4-(trifluoromethyl)benzaldehyde with HBPin to give boronate ester **x** under optimized conditions.

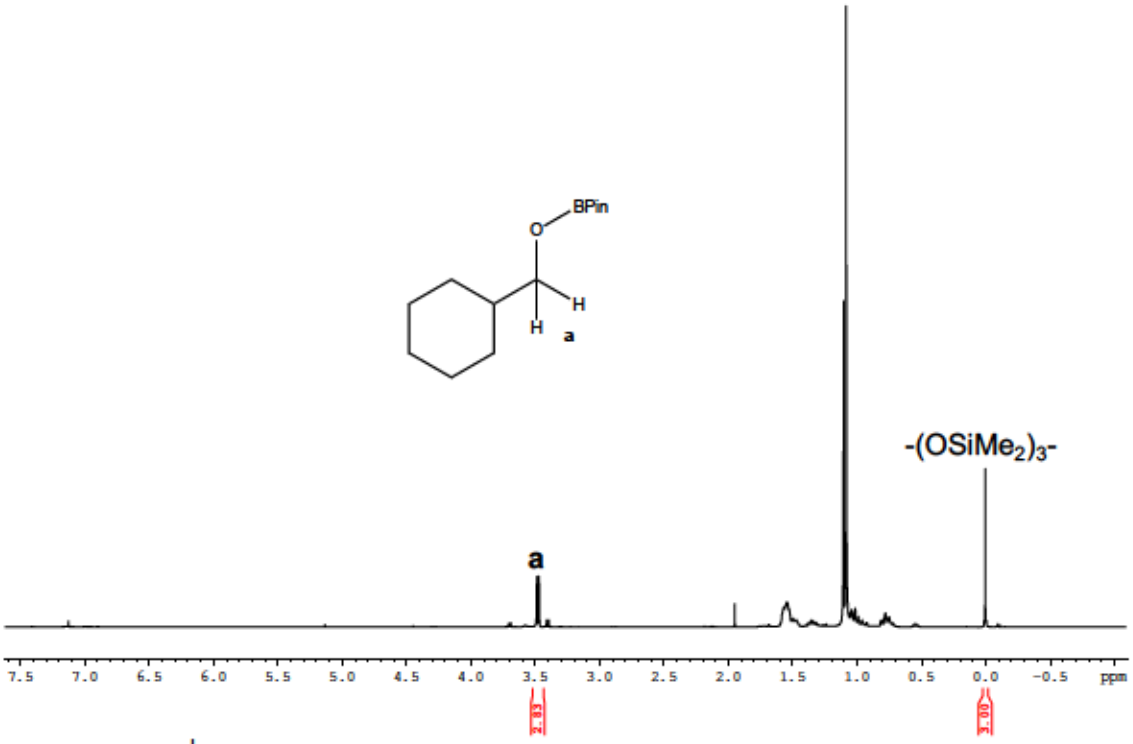

Figure S22. ^{1}H NMR spectra of the reaction products of the hydroboration of cyclohexanecarboxaldehyde with HBPin to give boronate ester **xi** under optimized conditions.

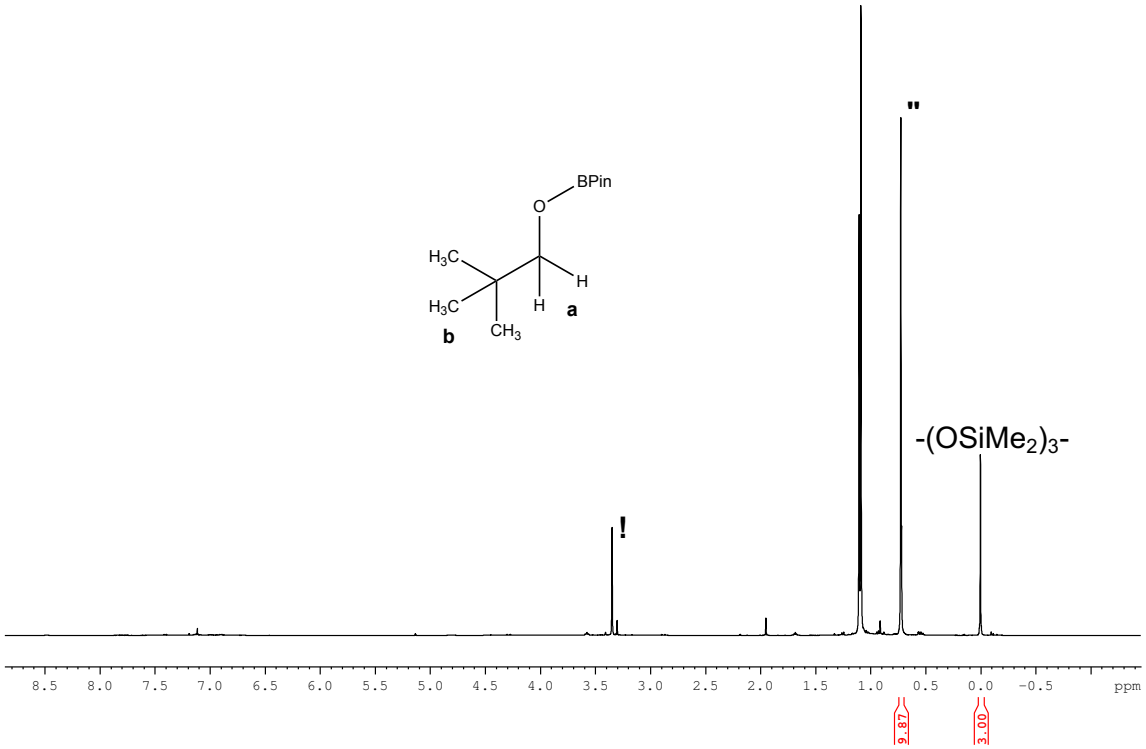

Figure S23. ^{1}H NMR spectra of the reaction products of the hydroboration of trimethylacetaldehyde with HBPin to give boronate ester **xii** under optimized conditions.

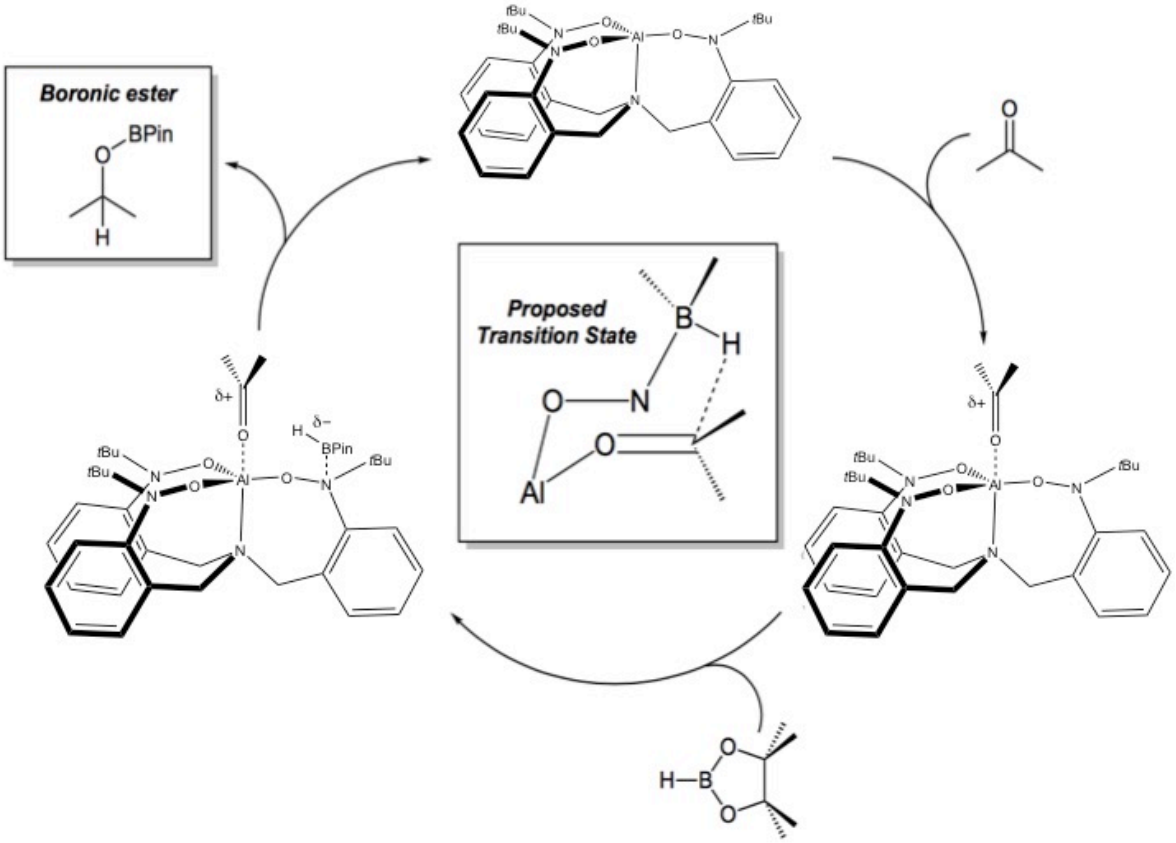

Scheme S1. Proposed catalytic cycle for the (TriNOx^{3-})Al-catalyzed carbonyl hydroboration.

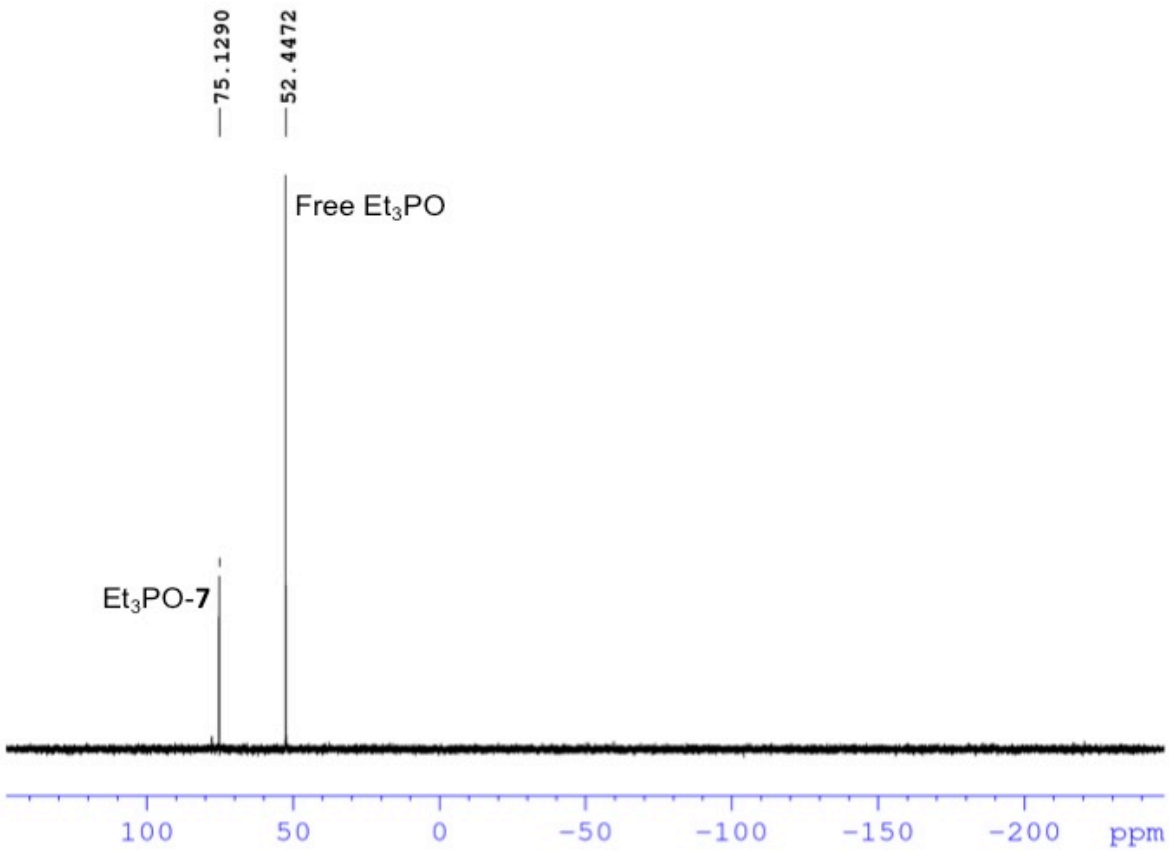

Figure S24. $^{31}P\{^{1}H\}$ NMR spectra of mixture of (TriNOX^{3-})Al and Et_3PO in $CDCl_3$ used to calculate the AN of the (TriNOx^{3-})Al complex.

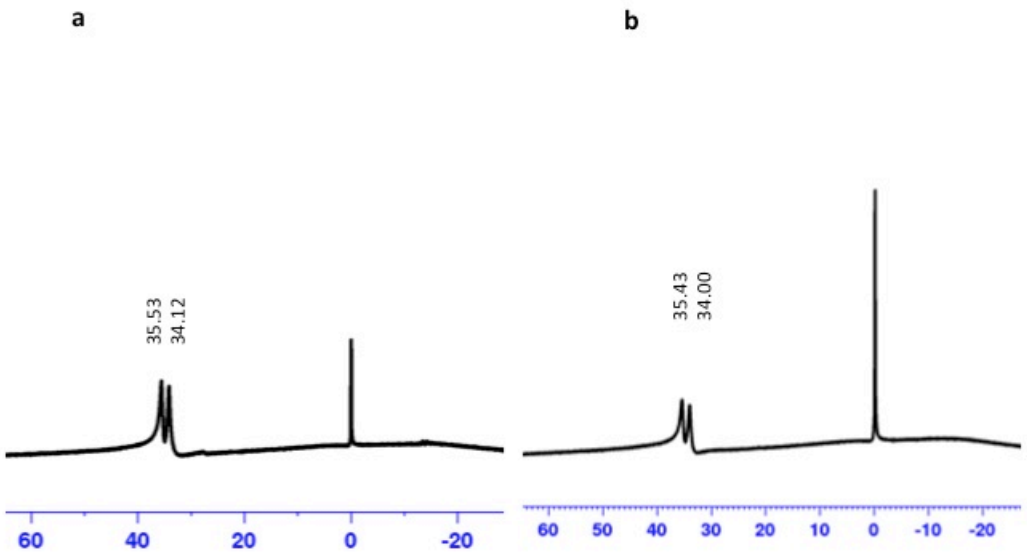

Figure S25. ^{11}B NMR spectra of HBPin (a) and the HBPin/(TriNOx^{3-})Al mixture (b) in $CDCl_3$ referenced to [*n*-Pr_4N][BAr^F].

References

(1) Morrish R. Bullock. *Catalysis Without Precious Metals*; Wiley-VCH Verlag GmbH & Co, 2010.

(2) Daniel Rabinovich. The Allure of Aluminum. *Nat. Chem.* **2013**, *76* (5).

(3) Element Facts https://www.chemicool.com (accessed Dec 11, 2018).

(4) Inukai, T.; Kasai, M. Diels—Alder Reactions of Acrylic Acid Derivatives Catalyzed by Aluminum Chloride. *J. Org. Chem.* **1965**, *30* (10), 3567–3569. https://doi.org/10.1021/jo01021a508.

(5) Meeks, B. S.; Lucas, A. R. Friedel Crafts Alkylation Using Elemental Aluminum Catalyst: An Undergraduate Laboratory Experiment. *J. Chem. Educ.* **1989**, *66* (2), 176. https://doi.org/10.1021/ed066p176.

(6) Murthy, J. K.; Gross, U.; Rüdiger, S.; Rao, V. V.; Kumar, V. V.; Wander, A.; Bailey, C. L.; Harrison, N. M.; Kemnitz, E. Aluminum Chloride as a Solid Is Not a Strong Lewis Acid. *J. Phys. Chem. B* **2006**, *110* (16), 8314–8319. https://doi.org/10.1021/jp0601419.

(7) Halogenation of Benzene-The Need for a Catalyst. Chemistry LibreTexts December 18, 2013.

(8) A.L. Wilds. Reduction with Aluminum Alkoxides (The Meerwein-Ponndorf-Verley Reduction). Organic Reactions 1944.

(9) Berben, L. A. Catalysis by Aluminum(III) Complexes of Non-Innocent Ligands. *Chem. - Eur. J.* **2015**, *21* (7), 2734–2742. https://doi.org/10.1002/chem.201405400.

(10) Lyaskovskyy, V.; de Bruin, B. Redox Non-Innocent Ligands: Versatile New Tools to Control Catalytic Reactions. *ACS Catal.* **2012**, *2* (2), 270–279. https://doi.org/10.1021/cs200660v.

(11) Sinha, S.; Das, S.; Sikari, R.; Parua, S.; Brandaõ, P.; Demeshko, S.; Meyer, F.; Paul, N. D. Redox Noninnocent Azo-Aromatic Pincers and Their Iron Complexes. Isolation, Characterization, and Catalytic Alcohol Oxidation. *Inorg. Chem.* **2017**, *56* (22), 14084–14100. https://doi.org/10.1021/acs.inorgchem.7b02238.

(12) Ciccione, J.; Leconte, N.; Luneau, D.; Philouze, C.; Thomas, F. Geometric and Electronic Structures of Nickel(II) Complexes of Redox Noninnocent Tetradentate Phenylenediamine Ligands. *Inorg. Chem.* **2016**, *55* (2), 649–665. https://doi.org/10.1021/acs.inorgchem.5b01947.

(13) Zuo, W.; Zhang, L.; Xie, M.; Deng, L. Square Planar Nickel(II) Complexes with Halogenated *o* -Diiminobenzosemiquinonato Ligation: Synthesis, Characterization, and Redox Property. *Chin. J. Chem.* **2013**, *31* (12), 1473–1482. https://doi.org/10.1002/cjoc.201300664.

(14) Myers, T. W.; Kazem, N.; Stoll, S.; Britt, R. D.; Shanmugam, M.; Berben, L. A. A Redox Series of Aluminum Complexes: Characterization of Four Oxidation States Including a Ligand Biradical State Stabilized via Exchange Coupling. *J. Am. Chem. Soc.* **2011**, *133* (22), 8662–8672. https://doi.org/10.1021/ja2015718.

(15) Koellner, C. A.; Piro, N. A.; Kassel, W. S.; Goldsmith, C. R.; Graves, C. R. Synthesis and Characterization of α-Diimine Complexes of Group 13 Metals and Their Catalytic Activity toward the Epoxidation of Alkenes. *Inorg. Chem.* **2015**, *54* (15), 7139–7141. https://doi.org/10.1021/acs.inorgchem.5b01136.

(16) Cole, B. E.; Wolbach, J. P.; Dougherty, W. G.; Piro, N. A.; Kassel, W. S.; Graves, C. R. Synthesis and Characterization of Aluminum-α-Diimine Complexes over

Multiple Redox States. *Inorg. Chem.* **2014**, *53* (7), 3899–3906. https://doi.org/10.1021/ic5003989.
(17) Schelter, E. J.; Wu, R.; Scott, B. L.; Thompson, J. D.; Cantat, T.; John, K. D.; Batista, E. R.; Morris, D. E.; Kiplinger, J. L. Actinide Redox-Active Ligand Complexes: Reversible Intramolecular Electron-Transfer in U(Dpp-BIAN)2/U(Dpp-BIAN)2 (THF). *Inorg. Chem.* **2010**, *49* (3), 924–933. https://doi.org/10.1021/ic901636f.
(18) Kraft, S. J.; Fanwick, P. E.; Bart, S. C. Synthesis and Characterization of a Uranium(III) Complex Containing a Redox-Active 2,2′-Bipyridine Ligand. *Inorg. Chem.* **2010**, *49* (3), 1103–1110. https://doi.org/10.1021/ic902008w.
(19) Heyduk, A. F.; Zarkesh, R. A.; Nguyen, A. I. Designing Catalysts for Nitrene Transfer Using Early Transition Metals and Redox-Active Ligands. *Inorg. Chem.* **2011**, *50* (20), 9849–9863. https://doi.org/10.1021/ic200911b.
(20) Berben, L. A.; de Bruin, B.; Heyduk, A. F. Non-Innocent Ligands. *Chem. Commun.* **2015**, *51* (9), 1553–1554. https://doi.org/10.1039/C4CC90480J.
(21) Khusnutdinova, J. R.; Milstein, D. Metal-Ligand Cooperation. *Angew. Chem. Int. Ed.* **2015**, *54* (42), 12236–12273. https://doi.org/10.1002/anie.201503873.
(22) Musa, S.; Shaposhnikov, I.; Cohen, S.; Gelman, D. Ligand-Metal Cooperation in PCP Pincer Complexes: Rational Design and Catalytic Activity in Acceptorless Dehydrogenation of Alcohols. *Angew. Chem. Int. Ed.* **2011**, *50* (15), 3533–3537. https://doi.org/10.1002/anie.201007367.
(23) Myers, T. W.; Berben, L. A. Aluminum–Ligand Cooperative N–H Bond Activation and an Example of Dehydrogenative Coupling. *J. Am. Chem. Soc.* **2013**, *135* (27), 9988–9990. https://doi.org/10.1021/ja4032874.
(24) Poitras, A. M.; Bogart, J. A.; Cole, B. E.; Carroll, P. J.; Schelter, E. J.; Graves, C. R. Synthesis and Characterization of Aluminum Complexes of Redox-Active Pyridyl Nitroxide Ligands. *Inorg. Chem.* **2015**, *54* (22), 10901–10908. https://doi.org/10.1021/acs.inorgchem.5b01941.
(25) Herb, T.M; Poitras, A.M; Richardson, K.G; Cole, B.E; Bogart, J.A; Carroll, B.E; Schelter, E.J; Graves, C.R. Synthesis and Characterization of Aluminum Nitroxide Complexes. *Polyhedron* **2016**, *114*, 194–199.
(26) Bogart, J. A.; Lippincott, C. A.; Carroll, P. J.; Schelter, E. J. An Operationally Simple Method for Separating the Rare-Earth Elements Neodymium and Dysprosium. *Angew. Chem. Int. Ed.* **2015**, *54* (28), 8222–8225. https://doi.org/10.1002/anie.201501659.
(27) Yang, Z.; Zhong, M.; Ma, X.; Nijesh, K.; De, S.; Parameswaran, P.; Roesky, H. W. An Aluminum Dihydride Working as a Catalyst in Hydroboration and Dehydrocoupling. *J. Am. Chem. Soc.* **2016**, *138* (8), 2548–2551. https://doi.org/10.1021/jacs.6b00032.
(28) Pang, M.; Wu, C.; Zhuang, X.; Zhang, F.; Su, M.; Tong, Q.; Tung, C.-H.; Wang, W. Addition of a B–H Bond across an Amido–Cobalt Bond: Co^{II} –H-Catalyzed Hydroboration of Olefins. *Organometallics* **2018**, *37* (9), 1462–1467. https://doi.org/10.1021/acs.organomet.8b00114.
(29) David A. Evans; Gregory C. Fu. The Rhodium-Catalyzed Hydroboration of Olefins: A Mechanistic Investigation. *J. Organomet. Chem.* **1990**, *55*.

(30) Gupta, M.; Mathur, P.; Butcher, R. J. Synthesis, Crystal Structure, Spectral Studies, and Catechol Oxidase Activity of Trigonal Bipyramidal Cu(II) Complexes Derived from a Tetradentate Diamide Bisbenzimidazole Ligand. *Inorg. Chem.* **2001**, *40* (5), 878–885. https://doi.org/10.1021/ic000313v.
(31) Bogart, J. A.; Cole, B. E.; Boreen, M. A.; Lippincott, C. A.; Manor, B. C.; Carroll, P. J.; Schelter, E. J. Accomplishing Simple, Solubility-Based Separations of Rare Earth Elements with Complexes Bearing Size-Sensitive Molecular Apertures. *Proc. Natl. Acad. Sci.* **2016**, *113* (52), 14887–14892. https://doi.org/10.1073/pnas.1612628113.
(32) Ogawa, A.; Fujimoto, H. Lewis Acidity of Gallium Halides. *Inorg. Chem.* **2002**, *41* (19), 4888–4894. https://doi.org/10.1021/ic020268m.
(33) Lin, T.-P.; Gabbaï, F. P. Two-Electron Redox Chemistry at the Dinuclear Core of a TePt Platform: Chlorine Photoreductive Elimination and Isolation of a Te^{V} Pt^{I} Complex. *J. Am. Chem. Soc.* **2012**, *134* (29), 12230–12238. https://doi.org/10.1021/ja3046074.
(34) Viktor Gutmann. Solvent Effects on the Reactivities of Organometallic Compounds. *Coord. Chem. Rev.* **1976**, No. 18, 225–255.
(35) M.A Beckett; G.C. Strickland; J.R. Holland; K.S. Varma. A Convenient NMR Method for the Measurement of Lewis Acidity at Boron Centers: Correlation of Reaction Rates of Lews Acid Initiated Epoxide Polymerizations with Lewis Acidity. *Polymer* **1996**, No. 37, 4629–4631.
(36) The Acceptor Number (AN) Was Calculated by the Gutmann−Beckett Method Using the Formula AN = 2.21 × (31LA·Et3PO − 41).
(37) Magritek. Determination of Lewis Acidity Using 31P NMR.
(38) Jakhar, V. K.; Barman, M. Kr.; Nembenna, S. Aluminum Monohydride Catalyzed Selective Hydroboration of Carbonyl Compounds. *Org. Lett.* **2016**, *18* (18), 4710–4713. https://doi.org/10.1021/acs.orglett.6b02310.
(39) Yang, Z.; Zhong, M.; Ma, X.; De, S.; Anusha, C.; Parameswaran, P.; Roesky, H. W. An Aluminum Hydride That Functions like a Transition-Metal Catalyst. *Angew. Chem. Int. Ed.* **2015**, *54* (35), 10225–10229. https://doi.org/10.1002/anie.201503304.
(40) Reactivity of Aldehydes and Ketones. Chemistry LibreTexts July 12, 2016.
(41) Wu, Y.; Shan, C.; Ying, J.; Su, J.; Zhu, J.; Liu, L. L.; Zhao, Y. Catalytic Hydroboration of Aldehydes, Ketones, Alkynes and Alkenes Initiated by NaOH. *Green Chem.* **2017**, *19* (17), 4169–4175. https://doi.org/10.1039/C7GC01632H.
(42) Corey, E. J.; Helal, C. J. Reduction of Carbonyl Compounds with Chiral Oxazaborolidine Catalysts: A New Paradigm for Enantioselective Catalysis and a Powerful New Synthetic Method. *Angew Chem Int Ed* **1998**, 27.
(43) R. K Thomason; B.L. Scott; D.E. Morris; J.L. Kiplinger. Synthesis, Structure, Spectroscopy and Redox Energetics of a Series of Uranium (IV) Mixed-Ligand Metallocene Complexes. *C.R.Chim.* No. 13, 790–802.
(44) APEX II, v. 2012.10-0 or v. 2013.4-1; Bruker AXS: Madison, WI, 2012.
(45) Bruker SAINT, v8.37a; Bruker AXS Inc.: Madison, WI, 2012.
(46) Sheldrick, G. M. SHELXL. Acta Crystallogr., Sect. C: Struct. Chem. 2015, C71, 3−8.
(47) Sheldrick, G. M. SADABS; University of Göttingen: Göttingen, Germany, 2007.

(48) Sheldrick, G. M. SHELXT. Acta Crystallogr., Sect. A: Found. Adv. 2015, A71, 3−8.
(49) Sheldrick, G.M. Acta Cryst. 2008, A64,112-122.